Parameterization of the Bulk Effects of Lateral and Cloud-Top Entrainment in Transient Shallow Cumulus Clouds

KNUT VON SALZEN AND NORMAN A. MCFARLANE

Canadian Centre for Climate Modelling and Analysis, Meteorological Service of Canada, University of Victoria, Victoria, British Columbia, Canada

(Manuscript received 13 September 2000, in final form 9 May 2001)

ABSTRACT

A parameterization of shallow cumulus clouds for use in atmospheric general circulation models is proposed. The parameterization uses a bulk representation of an ensemble of transient clouds. Entrainment of environmental air occurs at the ascending top of the cumulus cloud and also at the lateral boundaries of the region below the top of the cloud. Complete detrainment of the air in the cloud occurs when the top of the cloud reaches its maximum height, chosen to be the level of neutral buoyancy. The parameterization is calibrated using results from the undisturbed period of the Barbados Oceanographic and Meteorological Experiment (BOMEX). Vertical profiles of in-cloud properties and mass fluxes obtained from large eddy simulations (LES) for the undisturbed BOMEX period are successfully reproduced by the parameterization. Good agreement is also found in comparisons with large-scale heat and moisture budgets diagnosed from observations during the same period of the experiment. However, this is achieved with a different choice for the parameters of the scheme.

1. Introduction

Over large areas in the subtropics and Tropics, the vertical redistribution of boundary layer air in shallow cumulus clouds represents an important source of heat and moisture in the lower troposphere. Nitta and Esbensen (1974) and Ciesielski et al. (1999) attribute apparent heat sinks on the order of 4 K day^{-1} and apparent moisture sources on the order of about 3 to 6 g kg^{-1} day^{-1} in the Atlantic trade wind regime primarily to detrainment of shallow clouds near the trade wind inversion layer. Episodic trade wind regimes over the western Pacific warm pool are frequent enough to impact heating and moistening budgets and may be important in the formation of deep convective clouds (Johnson and Lin 1997). Apparently there is a need to take into account the effects of shallow cumulus clouds in atmospheric general circulation models (AGCMs) used in climate change studies and for weather prediction. Additionally, small cumulus clouds can be expected to be relevant to air chemistry and aerosol research owing to efficient entrainment and mixing of chemical species from the lower troposphere and negligible scavenging of chemical reaction products by precipitation.

Corresponding author address: Dr. K. von Salzen, Canadian Centre for Climate Modelling and Analysis, Meteorological Service of Canada, University of Victoria, P.O. Box 1700, STN CSC, Victoria, BC V8W 2Y2, Canada.
E-mail: knut.vonsalzen@ec.gc.ca

As is well known, AGCMs are typically designed to resolve processes with horizontal scales of a few hundred kilometers, vertical scales of tens to hundreds of meters and temporal scales of hours and longer. While it is true that the actual time step length in many such models is only a few minutes, this is mainly for computational reasons and it is not uncommon to impose periodic or continuous temporal smoothing of prognostic variables using filtering operators to prevent development of undesirable fluctuations at the highest resolved frequencies (Asselin 1972). Thus the major problem associated with the treatment of convective clouds in AGCMs is that individual convective elements, and even organized convective systems, have characteristic temporal and spatial scales that are much smaller than those usually resolved by these models. Thus as in most parameterization problems, the most important net effects of moist convection must be represented in AGCMs in an appropriately averaged way.

Research on simplified representations of the basic processes in cumulus clouds that are relevant to large-scale modeling has been active for several decades. Various, often substantially different, parameterizations of the effects of convective clouds have been suggested and used to account for the effects of shallow convection in large-scale models. For example, adjustment schemes are based on the principle that convection acts to adjust the larger-scale atmospheric state toward one that is neutrally stable and/or consistent with observed structures in the Tropics (Betts 1986).

Many of the parameterizations in current use are based on the mass flux approach wherein vertical fluxes of such quantities as mass, heat, moisture, and other prognostic scalars associated with convective clouds are represented using simple cloud models, often based on the entraining plume concept (e.g., Tiedtke 1989). However, both observations and modeling of properties of cumulus clouds within the last 3 decades have raised doubts about the validity of the entraining plume concept as a model of shallow cumulus clouds. Observational studies from a wide range of field experiments suggest that the distribution of cloud properties at any given level in individual cumulus clouds is typically nonhomogeneous and may be comprised of mixtures of air parcels that have entered the cloud from many different levels in the convective layer, including air from environmental levels up to a few hundred meters above the level of observation (Paluch 1979; Blyth et al. 1988). For the most part these observations are inconsistent with the entraining plume concept and this has motivated introduction of the concepts of episodic entrainment (Raymond and Blyth 1986) to explain the observations. Associated conceptual models such as the shedding thermal model (Blyth et al. 1988; Blyth 1993) have been proposed as a mechanism for such entrainment and mixing processes to occur in clouds. In this model entrainment occurs in and around thermals in the rising tops of cumulus clouds. These thermals shed cloudy air in their wake. Updrafts and downdrafts and turbulence would typically also occur in the cloudy wake region and this could in principle result in further entrainment and detrainment. However, most of the available observations suggest that the properties of the air throughout the cloud remains nonhomogeneous and often gives the appearance of being comprised of mixtures of air from near or above the ambient level and almost undiluted air from the vicinity of the cloud-base region. Results of Blyth et al. (1988) for small Montana cumuli and other observations (e.g., Stith 1992) are consistent with this schematic model. Recent simulations with cloud resolving models such as those of Carpenter et al. (1998) lend some support to the shedding thermal concept, although there does not appear to be substantial support for this concept from laboratory studies (Morton 1997).

Whether in association with the circulation around thermals or in some other way, episodic entrainment and associated mixing can explain how cloudy air at a given level would appear to be comprised of mixtures of environmental air from above or near the observation level and air from lower levels, including the cloud-base region. However, there is also evidence that observed departures from such mixing line structures may be associated with buoyancy sorting (Taylor and Baker 1991) such that individual cloudy parcels may, after the initial mixing associated with episodic entrainment, remain sufficiently distinct to ascend or descend to levels in the cloud where they are neutrally buoyant with respect the the cloud-free environment. The episodic mixing and buoyancy sorting hypotheses are central to the parameterization schemes of Raymond and Blyth (1986) and Emanuel and Živković-Rothman (1999). These authors assume that environmental air is mixed into a cumulus cloud in such a way as to give rise to a spectrum of air parcels with different mixing fractions within the cloud. These parcels then ascend or descend toward levels of neutral buoyancy. While these parameterizations are conceptually in better agreement with the aforementioned observations of cumulus clouds than are entraining plume models, the plume models do permit realistic representation of some key features of cumulus clouds in a simple way. For example Raga et al. (1990) found that the mean thermodynamic properties and mass flux in much of the cloud layer for Hawaiian trade wind cumuli could be represented with reasonable accuracy using an entraining plume model. However, significant departures from the entraining plume model predictions occur in the upper portion of the cloud layer.

While it is difficult to summarize the details of the life cycle of small cumulus clouds, there are observations and model results that suggest a relatively short and pronounced collapse phase near the end of the life cycle of small cumuli. For example, vertical mass fluxes of Hawaiian trade wind cumuli derived from dual-Doppler radar observations are characterized by rapid decay within a small fraction of the total cloud lifetime (Grinnell et al. 1996). Distinct decay of cloud properties may be attributable to penetrative downdrafts (Squires 1958) that form in the upper portions of clouds as a result of collapsing turrets and evaporative cooling. According to the model results of Carpenter et al. (1998), the narrowest and strongest downdrafts in a cloud develop in the later stages of the life cycle along the edges of ascending turrets that overshoot their level of neutral buoyancy (LNB). Raga et al. (1990) came to similar conclusions in an earlier and different study.

As noted above, parameterizations of shallow moist convection that are based on the steady entraining plume concept are currently in wide use in AGCMs. In these parameterizations, the in-cloud properties in individual plumes are generally assumed to be homogeneously distributed at each level. Thus they are conceptually in basic disagreement with many of the aforementioned observations within convective clouds. Another shortcoming of most current entraining plume parameterizations is the assumption of steady-state clouds. Betts (1975), Fraedrich (1974), and Cho (1977) have discussed the effects of accounting for recycling of cloudy air into the environment as cumulus clouds decay. The work of Fraedrich (1974) in particular generalized to some extent the earlier work of Kuo (1965). Including such effects can in principle account for important aspects of the observed large-scale moistening of the convective layer that occurs in association with shallow cumulus activity and the basic features of the observed cooling in the upper parts of the convective layers. How-

ever, these studies do not take into explicit account the effects of nonhomogeneity in cloud properties and make ad hoc assumptions about the recycling rate and/or the properties of the recycled air in order to obtain a closed form parameterization or deduce it from observed heat and moisture budgets. In order to account for cumulus life cycle effects in the context of steady entraining plume models it is also necessary to introduce ad hoc assumptions concerning detrainment processes (Siebesma and Holtslag 1996) or to employ a spectral cumulus ensemble model with component plumes having different entrainment characteristics as in Arakawa and Schubert (1974). Although an appropriate choice of the elements of the ensemble results in realistic simulations of the effects of convective clouds (Lin and Arakawa 1997b) it does not address the inherent limitations of the steady entraining plume model and requires introduction of additional closure conditions.

The motivation for the development of the parameterization presented in this paper is to account for the combined effects of inhomogeneities in the horizontal distributions of in-cloud properties and of finite cumulus lifetimes by generalizing the earlier approach of Fraedrich (1974). As in that approach and the earlier one of Kuo (1965) it is assumed that individual cumulus clouds grow until they reach their maximum heights and then rapidly decay with an associated lateral mixing of cloud properties into the environment. However, as important generalizations, we will account for nonhomogeneity in cloud properties arising from entrainment of environmental air in narrow regions near the rising tops of cumulus clouds and we will also derive a self-consistent expression for the detrainment associated with recycling of cloudy air at the ends of cumulus life cycles. Since our goal is to represent the time-averaged (over cumulus life cycles) effects of shallow cumulus clouds we will employ an idealized representation of cumulus clouds in which cloud properties are assumed to be steady except near the rising tops of the cumuli.

First tests and applications of the new parameterization are discussed in this paper. The parameterization is calibrated and characteristic features are investigated using prescribed vertical profiles of environmental temperature and water vapor mixing ratios from phase 3 (22 to 30 June 1969) of the Barbados Oceanographic and Meteorological Experiment (BOMEX; Holland and Rasmusson 1973). Comparisons are done for results from large eddy simulations (LES) and large-scale heat and moisture budgets derived from observations (Nitta and Esbensen 1974). In order to put the results of the new parameterization into broader perspective, we also discuss comparisons with the results of using the modified version of the Tiedtke (1989) parameterization proposed by Siebesma and Holtslag (1996).

2. Basic model of transient shallow cumulus clouds

The basic concept of the proposed parameterization is illustrated in Fig. 1. A cumulus cloud is initiated by turbulent processes in a conditionally unstable planetary boundary layer by lifting of air parcels from the mixed layer into the cloud layer where, under favorable conditions, the water vapor in the parcels becomes saturated and condensation occurs with continued ascent. Upon reaching the level of free convection (LFC), the cloud which forms ascends under the action of buoyancy forces. The buoyancy and other in-cloud properties are strongly affected by entrainment and detrainment processes at the top and sides of the rising cloud. To account for this we will introduce separate representations for mass entrainment rates at the rising top (E_i and D_i) and those at the sides of the cloud below the rising top (E_s and D_s).

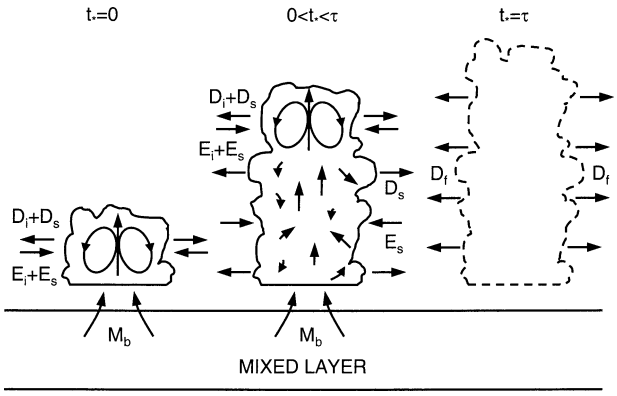

FIG. 1. Simplified life cycle of a shallow cumulus cloud. The cloud begins to form at time $t_* = 0$ and collapses at $t_* = \tau$. The air in the cloud is modified by entrainment and detrainment at the top of the cloud (E_i and D_i) and at the lateral boundaries (E_s and D_s). Final and complete detrainment (D_f) occurs at $t_* = \tau$.

The cloud top finally arrives at its maximum height near the level of neutral buoyancy. The ascent of the cloud top above the LNB is inhibited by the decrease in buoyancy, leading to the formation of penetrative downdrafts as illustrated by model results by Carpenter et al. (1998). We assume that these processes lead to a rapid decay of the cloud as suggested by observed vertical cloud mass fluxes by Grinnell et al. (1996). This decay process is simply approximated as an abrupt lateral detrainment of cloudy air into the environment (D_f in Fig. 1) at the end of the growth cycle of the cloud. In reality the mixing of cloudy and environmental air in a decaying cloud would likely result in the formation of negatively buoyant mixtures that may then sink within the cloud before entering the environment. While doing so it is also possible that descending parcels may undergo further mixing with other cloudy parcels before finally entering the environment. These processes are ignored for the sake of simplicity in the parameterization of shallow convection that is developed here. The observations of Blyth et al. (1988) and the modeling results of Carpenter et al. (1998) and Lin and Arakawa (1997a) suggest that negatively buoyant cloud air parcels usually descend less than a few hundred meters during the cloud

life cycle. However, ignoring the final buoyancy sorting phase that may take place before cloudy air is recycled into the environment results in important differences between the simple parameterization that is developed here and those that attempt to account for the main effects of buoyancy sorting (Raymond and Blyth 1986; Emanuel 1991; Emanuel and Živković-Rothman 1999).

As noted in the introduction, the intent of the parameterization that is developed here is to account for the effects of shallow cumulus clouds on the larger-scale environment in terms of averages over the life cycles of individual clouds. To begin with we will introduce a mathematical description of the simplified cloud life cycle model that is the basis of the parameterization. As will be seen, the simplifying assumptions introduced below give rise to an easily interpreted and implemented mathematical representation of the time-averaged effects of shallow cumulus clouds.

a. Basic model equations

The fundamental set of equations of the parameterization consists of continuity equations for mass, general scalar properties χ, and vertical momentum in the convectively active region. The introduction of a fractional cloud cover a, the ratio of the cloudy to the total area, leads to time-dependent equations for these quantities in the convectively active part of the cloud. Using the anelastic form of the governing equations, these are (Arakawa and Schubert 1974; Siebsma 1998)

$$\rho\frac{\partial a}{\partial t} = -\frac{\partial}{\partial z}(\rho a w_c) + E - D, \tag{1}$$

$$\rho\frac{\partial}{\partial t}(a\chi_c) = -\frac{\partial}{\partial z}(\rho a\overline{w\chi}^c) + E\chi_e - D\chi_c + \rho a S_\chi, \tag{2}$$

$$\rho\frac{\partial}{\partial t}(aw_c) = -\frac{\partial}{\partial z}(\rho a\overline{w^2}^c) - Dw_c + \rho a\frac{B_c}{1+\gamma} - \frac{\partial}{\partial z}(aP_c), \tag{3}$$

where ρ is the background density of the air and w the vertical velocity. The subscript c refers to quantities averaged over the cloudy region. The index e refers to quantities averaged over the environment of the convectively active region. Due to typically small values of a, χ_e is approximately given by the average over the entire domain, including clouds. Overbars in Eqs. (1) to (3) denote averages of derived quantities, such as the average vertical flux of χ, $\rho\overline{w\chi}^c$, and the vertical momentum flux $\rho\overline{w^2}^c$ in the cloudy region. The exchange of mass between cumulus clouds and the environment is represented in terms of the entrainment rate, E, and detrainment rate, D.

In the continuity equation for scalar properties χ, Eq. (2), $E\chi_e$ refers to entrainment from the environment into the cloud, $D\chi_c$ refers to detrainment of the cloud into the environment, and S_χ denotes in-cloud sources and sinks of χ. The scalar variables governed by Eq. (2) that are considered are the total water mixing ratio r_t and the moist static energy $h = c_pT + L_vr + gz$, where c_p is the specific heat at constant pressure for dry air, T the temperature of the air, L_v the latent heat of vaporization, r the water vapor mixing ratio, g the gravitational acceleration, and z the height. Effects of drizzle and radiation on small cumuli are usually small (e.g., Jiang and Cotton 2000) and the last term in Eq. (2) is omitted for r_t and h in the following.

The vertical momentum budget in Eq. (3) includes terms which refer to detrainment of horizontally averaged vertical velocity w_c, production of vertical momentum by buoyancy B_c, and effects of pressure perturbations P_c inside the cloud. No entrainment of vertical momentum is considered since it is assumed that vertical velocities are small in the environment compared to velocities in the cloud.

The mean perturbation pressure quantity P_c is retained to account for the dynamical response of the pressure field to horizontal inhomogeneity in the cloud vertical velocity field. This quantity is discussed further below but it should be noted that it does not account for all of the components that may be important in the pressure gradient force. As discussed by Yau (1979), the pressure gradient force in simple cumulus cloud models should typically have a component that partially offsets the buoyancy force and a dynamical component that is associated with the velocity field within the cloud. These two components are not distinguished here except for the part of the dynamical component that arises in response to the occurrence of inhomogeneity in the vertical velocity as indicated above. It is assumed that this dynamical component vanishes near the edge of the cloud. The reduction of the buoyancy force due to the pressure gradient force is accounted for in terms of a virtual mass parameter γ in the buoyancy term in Eq. (3), as is typical in one-dimensional cumulus models (e.g., Simpson and Wiggert 1969). The value of this parameter will be derived from results of LES models in section 3.

The buoyancy in Eq. (3) is calculated at each level in the cloud from the horizontally averaged virtual temperature T_{vc} in the cloud and the virtual temperature of environmental air T_{ve},

$$B_c = g\frac{T_{vc} - T_{ve}}{T_{ve}}, \tag{4}$$

where the virtual temperature is given approximately by

$$T_v = T(1 + 0.608r_t - 1.608r_l),$$

with the liquid water mixing ratio r_l.

b. Cloud life cycle

Note that the fractional cloud cover is a factor in all terms involving temporal and vertical derivatives in the

above equations. In order to obtain a simple representation of cloud life cycle effects we assume that all cloud properties are steady except within a narrow region in the vicinity of the rising top. Thus all cloud properties undergo jumplike transitions from environmental to (quasi-steady) in-cloud values at the rising cloud top. Because of the way in which the fractional cloud cover appears in the above equations this assumption can be accommodated in a simple way by assuming that only the fractional area, detrainment and entrainment terms are explicit functions of time. We define the dimensionless cloud cover a as that portion of the cumulus layer that has a nonvanishing liquid water content (LWC), that is it represents the visible clouds in the domain. Thus it is assumed that the temporal variability of the fractional area a is confined to a narrow region near the rising top and this quantity is represented in terms of the difference of two Heaviside step functions as

$$a(z, t) \equiv a_0(z)\left[H\left(\frac{t - t_*(z)}{\tau}\right) - H\left(\frac{t - \tau}{\tau}\right)\right], \quad (5)$$

where $a_0(z)$ is the steady part of fractional cloud cover. It will be shown later that this parameter is entirely defined by the solutions of Eqs. (1) and (3) for a defined by Eq. (5).

For simplicity and without loss of generality we assume that the cloud begins its life cycle at time $t = 0$. The first Heaviside function in the square brackets in Eq. (5) represents the expansion of the cloud volume due to an ascending cloud top, the second represents the collapse of the cloud at $t = \tau$ at the time the ascending cloud top reaches its maximum height at $z = z_t$. In Eq. (5), t_* is the time elapsed between inception and the time at which the cloud reaches a certain height. Thus, because of the definition of the Heaviside function (zero when its argument is negative, unity otherwise), the fractional area and hence the mean vertical mass flux ($M_c = \rho a w_c$) is nonzero only for $t_* \leq t \leq \tau$. Within this time period, however, it is assumed to be steady. As will be seen later, this fact has an important bearing on the form of the time-averaged mass flux.

The entrainment and detrainment rates at cloud top and an equation for t_* are given below. In order to determine these quantities it is necessary to account for the role of spatial inhomogeneity within the rising cloud.

c. Effects of subcloud variability on vertical fluxes

Observed inhomogeneities in the horizontal distribution of conserved properties and vertical velocities in shallow clouds imply that the horizontally averaged vertical flux of a scalar χ at a specific level in a cloud generally decomposes into cloud mean and sub-cloud-scale parts; that is,

$$\overline{w\chi}^c = w_c\chi_c + \overline{w'\chi'}^c, \quad (6)$$

where the prime denotes a deviation from the horizontal average over the cloudy region.

We propose a simple parameterization of the sub-cloud-scale contribution in terms of cloud-scale variables,

$$\overline{w'\chi'}^c = \alpha w_c(\chi_c - \chi_e). \quad (7)$$

The limiting case $\alpha = 0$ refers to top-hat distributions of the in-cloud properties. The magnitude of α is determined by the efficiency of the mixing processes to produce nonuniform distributions of the scalar properties in the cloudy region below the advancing cloud top. This parameter can be calculated from Eqs. (6) and (7) by use of the hypothesis that all mixtures at a particular level in a cloud lie along the mixing line for mixtures of environmental air drawn into the cloud by entrainment and air within the cloud that has entered at lower levels. In the absence of lateral entrainment below the rising top of the cloud this cloudy air would typically have originated at cloud base. Thus any conserved quantity χ in the cloud is represented as

$$\chi = \tilde{\chi} + f(\chi_e - \tilde{\chi}), \quad (8)$$

where f is the fraction of environmental air in a linear mixture of χ_e and $\tilde{\chi}$. We will choose $\tilde{\chi}$ to be such that α depends only on the mean value of the mixing fraction in the cloud. This is achieved by choosing it such that

$$w_c\tilde{\chi} \equiv \overline{w\chi}^c. \quad (9)$$

It follows directly that α can be expressed by

$$\alpha = \frac{f_c}{1 - f_c}. \quad (10)$$

Here f_c is the horizontally averaged value of f in the cloud at a given level; f_c depends on the probability density distribution $p(f)$ of f in the cloud and is given by

$$f_c = \int_0^{f_{\max}} fp(f)\, df, \quad (11)$$

where $f_{\max}$ refers to the most diluted air in the cloud, which is assumed to occur predominantly near the edge of the visible cloud where its liquid water content is negligible. An efficient method for the calculation of $f_{\max}$ is presented in appendix A.

It is easily shown that the relationship between α and f_c implies that

$$\rho\overline{wf}^c = 0,$$

and hence that in general there must be both updrafts and downdrafts within the cloud.

While $p(f)$ in Eq. (11) can in principle be derived from observations or cloud resolving model simulations, there is to our knowledge no published data on probability distributions of mixing fractions for shallow cumulus clouds. In order to obtain a sufficiently general parameterization of α for use in an AGCM, it would be necessary to specify the statistical quantities at different

stages of the life cycles for many individual clouds. The alternative that is used in this study is to introduce physical assumptions and to test the sensitivity of ensemble-mean cloud properties and fluxes to these assumptions in the context of the BOMEX experiment. The probability density distributions that are used in associated sensitivity tests are described in section 3.

d. Solutions of basic equations

In the following, the approaches presented above are used to solve the fundamental set of equations of the parameterization [Eqs. (1) through (3)].

Because the assumed abrupt onset of the cloud at time t_* and cessation at $t = \tau$ is represented in terms of Heaviside functions [Eq. (5)], the vertical and temporal derivatives of these functions can consistently be represented in terms of Dirac delta functions. Entrainment and detrainment processes near the rising cloud top and the final detrainment are also represented in terms of delta functions. Those occurring below cloud top are represented, similarly to the fractional area, in terms of the difference between the Heaviside functions representing the initiation and cessation of the cloud at a given height. Thus we assume that

$$E = E_i\delta\left(\frac{t - t_*(t)}{\tau}\right) + E_s\left[H\left(\frac{t - t_*(z)}{\tau}\right) - H\left(\frac{t - \tau}{\tau}\right)\right],$$

$$D = D_i\delta\left(\frac{t - t_*(z)}{\tau}\right) + D_s\left[H\left(\frac{t - t_*(z)}{\tau}\right) - H\left(\frac{t - \tau}{\tau}\right)\right] + D_f\delta\left(\frac{t - \tau}{\tau}\right).$$

Inserting these expressions and the expressions for a [Eq. (5)] into Eqs. (1) through (3) and equating coefficients of Dirac and Heaviside functions to zero gives the following:

$$D_f = \frac{\rho a_0}{\tau}, \tag{12}$$

$$D_i - E_i + \frac{\rho a_0}{\tau}\left(1 - w_c\frac{dt_*}{dz}\right) = 0, \tag{13}$$

$$D_i\chi_c - E_i\chi_e + \frac{\rho a_0}{\tau}\left(\chi_c - \frac{dt_*}{dz}w_c\tilde{\chi}\right) = 0, \tag{14}$$

$$D_i w_c + \frac{\rho a_0}{\tau}\left[w_c - \frac{dt_*}{dz}\left(\overline{w^2}^c + \frac{P_c}{\rho}\right)\right] = 0, \tag{15}$$

$$D_s - E_s + \frac{\partial}{\partial z}(\rho a_0 w_c) = 0, \tag{16}$$

$$D_s\chi_c - E_s\chi_e + \frac{\partial}{\partial z}(\rho a_0 w_c\tilde{\chi}) = \rho a_0 S_\chi, \tag{17}$$

$$D_s w_c + \frac{\partial}{\partial z}(\rho a_0\overline{w^2}^c + a_0 P_c) = \frac{\rho a_0 B_c}{1 + \gamma}. \tag{18}$$

Combining Eqs. (13) and (14) using Eqs. (6), (7), and (9) leads to the following expressions for the cloud-top entrainment and detrainment terms:

$$E_i = \frac{\rho a_0}{\tau}\alpha w_c\frac{dt_*}{dz}, \tag{19}$$

$$D_i = \frac{\rho a_0}{\tau}\left[(1 + \alpha)w_c\frac{dt_*}{dz} - 1\right]. \tag{20}$$

Equation (15) then gives

$$\frac{P_c}{\rho} + \overline{w^2}^c = (1 + \alpha)w_c^2.$$

This result, substituted in Eq. (18), gives an equation for the mean vertical velocity in the cloud as

$$D_s w_c + \frac{\partial}{\partial z}[(1 + \alpha)\rho a_0 w_c^2] = \rho a_0\frac{B_c}{1 + \gamma}. \tag{21}$$

In order to determine t_*, an additional relationship concerning detrainment and/or entrainment at cloud top is required. One possible assumption is that the cloud top ascends at a rate given by the mean vertical velocity in the cloud so that

$$w_c\frac{dt_*}{dz} = 1.$$

In this case the rates of cloud-top entrainment and detrainment are equal to each other. Another possible assumption that we will examine is to ignore the detrainment at cloud top entirely. A heuristic justification for this may be that detrained air may be largely drawn back into the rising cloud-top region. The details of this process, if it occurs, are possibly too complicated to represent in a simplified way and therefore it may be worthwhile to simply ignore the cloud top detrainment process. Doing so gives

$$w_c\frac{dt_*}{dz} = \frac{1}{1 + \alpha}.$$

As will be demonstrated below, the results obtained when applying the parameterization are not very sensitive to the difference between these assumptions.

In order to determine $\tau = t_*(z_t)$, it is simply assumed that the collapse of the cloud is initiated at that time at which the ascending cloud top reaches its LNB at $z = z_t$. This assumption is consistent with the commonly used definition of the cloud top in the context of other parameterizations. However, this is not a necessary choice and other assumptions are in principle possible with regard to the application of the equations given above as long as $w_c > 0$ at $z = z_t$.

e. Organized entrainment and detrainment at lateral boundaries

Betts (1982) interpreted datasets by using convective pressure scales and saturation point coordinates. His re-

sults give evidence that the buoyancies of the air mixtures produced by cloud-top entrainment in typical trade wind cumulus regimes are too strong to produce downdrafts in clouds. To overcome this he suggests that a combination of cloud-top and lateral entrainment is required to explain up- and downdrafts in shallow clouds. The wide spread inclusion of lateral entrainment in entraining plume models stems from laboratory and field studies indicating the importance of lateral entrainment in penetrative convection.

Recent modeling studies give considerable insights into the nature of lateral entrainment and detrainment processes in shallow clouds (Bretherton and Smolarkiewicz 1989; Lin and Arakawa 1997a). Bretherton and Smolarkiewicz (1989) used a two-dimensional model to simulate an isolated long-lasting nonprecipitating cloud in a calm atmosphere with no surface forcing. Their results and an additional theoretical analysis show that lateral detrainment occurs preferably in regions with vertically decreasing buoyancy and entrainment in regions with increasing buoyancy in the cloud (Bretherton 1993). According to their results, buoyancy differences between cloud and the environment further away from the cloud produce circulations in the environment that tend to produce organized lateral flows toward the cloud in regions where the buoyancy increases with height and away from it where the buoyancy decreases with height.

A simple and pragmatic parameterization of organized lateral entrainment E_s and detrainment D_s mass fluxes that is consistent with the results of Bretherton and Smolarkiewicz has the form

$$\begin{pmatrix} E_s \\ D_s \end{pmatrix} = \rho a_0 w_c \begin{pmatrix} e \\ d \end{pmatrix}, \tag{22}$$

where the fractional entrainment and detrainment rates e and d are given by

$$\begin{pmatrix} e \\ d \end{pmatrix} = \mu \begin{pmatrix} \max\left(\dfrac{\partial B_u}{\partial z}, 0\right) \\ \max\left(-\dfrac{\partial B_u}{\partial z}, 0\right) \end{pmatrix}. \tag{23}$$

Here B_u denotes the buoyancy of the undiluted parcel that initiates the cloud.

The mixing rate scaling factor μ in Eq. (23) is a scalar that needs to be determined from closure assumptions. In our study, results from LES simulations and observations are used to determine μ.

f. Large-scale tendencies

The equations given in the previous sections are used to determine the mean effects of a shallow cumulus cloud ensemble on the large-scale environment. As noted in the introduction, these are expressed in terms of the time-averaged effects. The relevant expressions for these averages are derived in the appendix B, under the usual assumption that the horizontal extent of clouds is much smaller than that of the environment. The mean large-scale tendencies of h, r_t, and χ are generally defined by

$$\rho\left\langle\frac{\partial \chi_e}{\partial t}\right\rangle = -\frac{\partial}{\partial z}[\langle M_c\rangle(\tilde{\chi} - \chi_e)] + \rho\langle a\rangle S_\chi, \tag{24}$$

where the relevant time-averaged vertical mass flux $\langle M_c\rangle$ and fractional area $\langle a\rangle$ are

$$\langle M_c\rangle = M_0\left(1 - \frac{t_*}{\tau}\right), \tag{25}$$

$$\langle a\rangle = a_0\left(1 - \frac{t_*}{\tau}\right), \tag{26}$$

with $M_0 = \rho a_0 w_c$.

The quantities required to evaluate the right-hand side of Eq. (24) are obtained by combining Eqs. (8), (14), (16), and (21) to obtain the following equations:

$$\frac{\partial M_0}{\partial z} = (e - d)M_0, \tag{27}$$

$$\frac{\partial \tilde{\chi}}{\partial z} = (e - f_c d)(\chi_e - \tilde{\chi}) + \frac{S_\chi}{w_c}, \tag{28}$$

$$\frac{1}{2}\frac{\partial w_c^2}{\partial z} = (1 - f_c)\frac{B_c}{(1 + \gamma)} - w_c^2\left[e - f_c d + \left(\frac{1}{1 - f_c}\right)\frac{\partial f_c}{\partial z}\right]. \tag{29}$$

Equations (27) and (29) can be combined to obtain a_0 in Eq. (26).

3. Calibration and testing for the undisturbed BOMEX period

For calibration and testing of the new parameterization, results for the undisturbed period from 22 to 26 June 1969 during phase 3 of BOMEX are used. This period is characterized by little active deep cumulus convection (Nitta and Esbensen 1974). The BOMEX rawindsonde data and derived vertical heat fluxes indicate a transition to relatively active and organized convection after that period. The occurrence of a clear trade wind inversion, nearly steady-state conditions, and extensive observations are some of the features of this period that have been documented and studied in numerous scientific papers on the characteristics and effects of shallow clouds (e.g., Betts 1975; Soong and Ogura 1976; Esbensen 1978; Siebesma and Cuijpers 1995; Jiang and Cotton 2000).

The parameterization introduced in the previous section is applied to two independent data sets for the BOMEX experiment. The first dataset refers to results

of 6 LES models. The second dataset refers to the analysis of large-scale heating and moistening budgets of Nitta and Esbensen (1974).

The results of the LES models provide more detailed information about convective processes than is available from current analyses of the BOMEX observations such as that of Nitta and Esbensen (1974). Hence the time- and space-averaged results of the LES models are used to calibrate the parameterization. In detail, the calibration is performed for the treatment of cloud-top mixing [i.e., to determine $p(f)$, introduced in section 2c], and organized lateral mixing (i.e., to determine μ, introduced in section 2e). The results of the calibrated parameterization are then compared to additional LES results in order to evaluate its ability to consistently reproduce fluxes and cloud properties that are associated with active shallow cumulus in the LES simulations. Based on these results, the sensitivity of the results to the value of γ (section 2a) and to the treatment of cloud-top detrainment (section 2d) are studied.

The second important application of the parameterization involves direct comparison of the results of the parameterization and the analyzed large-scale heat and moisture budgets as determined by Nitta and Esbensen (1974).

For both datasets, the relationships given in the previous sections are used to diagnose the ensemble-mean shallow cumulus cloud fields and budgets that occurred during the undisturbed period of BOMEX. Other processes, such as turbulent diffusion in the boundary layer or cloud–radiation interactions, are not considered here.

a. Statistical distribution of cloud properties

Three versions of the parameterization are tested in order to study different limiting cases with regard to the treatment of cloud inhomogeneities.

The first and simplest of the cases is that the conserved in-cloud properties are top-hat distributed; that is, there is no horizontal variability in the cloud. Accordingly, there is no cloud-top entrainment and $p(f)$ [Eq. (11)] is simply a delta function, $p(f) = \delta(f)$. The version of the parameterization that corresponds to this assumption is labeled TOPHAT in the following in order to distinguish the results.

In the second case it is assumed that all mixtures have equal probabilities in the cloud at each level, that is the mixing fraction is uniformly distributed, which is expressed by $p(f) = f_{\max}^{-1}$. The corresponding version of the parameterization is labeled EQPROB.

Finally, in the third approach it is assumed that the probability of dilution for air in the top of the cloud increases with time as the cloud top ascends. At cloud base, the cloud properties are those of an undiluted parcel with the properties of air from the initial parcel launching level. Above cloud base, it is assumed that the cloud-top mixing acts in a way that it tends to produce a constant probability density distribution with time. As a first approximation, it is assumed that this process scales with t_{u*}, the time at which an undiluted parcel reaches a given height. The motivation for this approach is to include the average effects of the erosion of the core of the ascending cloud top as, for example, suggested in the schematic shedding thermal model proposed by Blyth et al. (1988). Since the details of the erosion process are not yet understood we may simply use

$$p(f) = \frac{\lambda \exp(-\lambda f)}{1 - \exp(-\lambda f_{\max})},$$

with

$$\lambda = \frac{\exp(-\varphi t_{u*})}{1 - \exp(-\varphi t_{u*})}.$$

With this approach, the magnitude of the cloud-top mixing depends on φ. The calibration of this parameter based on results for BOMEX is discussed in section 3c(1) below. The corresponding version of the parameterization for these assumptions is labeled DECORE.

b. Alternative parameterization of shallow cumulus

In order to evaluate the differences between the new approach and more traditional ones, the relatively simple entraining plume parameterization of Tiedtke (1989) is also considered in the context of the BOMEX results. The large-scale tendencies of general conserved scalar properties according to this parameterization are given by

$$\rho \frac{\partial \chi}{\partial t} = -\frac{\partial}{\partial z}[M_c(\chi_c - \chi_e)].$$

The mean vertical fluxes of mass M_c and conserved properties $M_c\chi_c$ are calculated from

$$\frac{\partial M_c}{\partial z} = E - D, \qquad \frac{\partial}{\partial z}(M_c\chi_c) = E\chi_e - D\chi_c,$$

corresponding to the assumption of top-hat distributed in-cloud properties. Life cycle effects are not considered.

The entrainment and detrainment fluxes in Tiedtke's parameterization are formulated in terms of the vertical mass flux; that is,

$$E = \epsilon_u M_c, \qquad D = \delta_u M_c.$$

Tiedtke (1989) uses fixed fractional entrainment and detrainment rates, given by $\epsilon_u = \delta_u = 3 \times 10^{-4}\ \mathrm{m}^{-1}$. Currently, various numerical weather prediction models and global circulation models use Tiedtke's parameterization in conjunction with these values. The general effect of the relatively small mixing rates in this approach is that undiluted air from cloud base represents a large fraction of the air in the parameterized shallow cumulus clouds. Consequently, detrainment of the air occurs predominantly at the top of the cloud layer, which

is given by the LNB. Siebesma and Holtslag (1996) concluded that for shallow cumulus cloud ensembles entrainment and detrainment rates are typically one order of magnitude larger than reported by Tiedtke (1989). They use LES results for the undisturbed BOMEX period to recalibrate Tiedtke's approach and show that values of $\epsilon_u = 2 \times 10^{-3}$ m^{-1} and $\delta_u = 2.7 \times 10^{-3}$ m^{-1} are in good agreement with the LES results. In this study, the approach suggested by Siebesma and Holtslag (1996, hereinafter referred to as SH1996) is used in comparisons with the new parameterization outlined in the previous sections.

c. Application to LES results

In this first study, data from an intercomparison project for LES models are used. This project was performed by members of the GEWEX Cloud System Studies (GCSS) Boundary Layer Cloud working group, one of the activities of the Global Energy and Water Cycle Experiment (GEWEX). In total 11 LES models from various international groups were applied to the period 22 to 23 June in BOMEX. Extensive results[1] for mass fluxes and cloud properties of clouds in the simulations have been presented at a group workshop from 24 to 25 July 1997 in Seattle, Washington (Siebesma et al. 2001, manuscript submitted to *J. Atmos. Sci.*; Siebesma and Cuijpers 1995). From the participating models, results of those 6 models are selected that are based on the Boussinesq approximation in order to be consistent with the current parameterizations. These 6 models are from the Royal Netherlands Meteorological Institute (KNMI; Cuijpers and Duynkerke 1993), the Max Planck Institute for Meteorology (MPI; Chlond 1992, 1994), the National Center for Atmospheric Research (NCAR; Moeng 1984, 1986), the Met Office (UKMO; MacVean 1993; Brown et al. 1994), the University of Oklahoma (UOK; Kogan et al. 1995), and the West Virginia University (WVU; Lewellen et al. 1996).

The size of the three-dimensional LES model domain is 6.4 km in both horizontal and 3 km in the vertical directions. The grid sizes are $\Delta z = 100$ m for the horizontal grid and $\Delta z = 40$ m for the vertical grid. Periodic boundary conditions are used at the lateral boundaries. A sponge layer above the inversion layer damps out any perturbations in the simulations. At the bottom, prescribed momentum, heat, and moisture fluxes are applied. Additional forcing in the simulations is applied with regard to large-scale subsidence, radiative cooling, and large-scale horizontal advection of moisture. The simulations are initialized with time-averaged vertical profiles of temperature and specific humidity that have been obtained by the *Oceanographer*, the ship at the northeast corner of the BOMEX domain. Random fluctuations of the virtual potential temperature and total water mixing ratio are used as initial perturbations at the lowest 40 levels. Hourly simulations results are available for a time period of 4 h after an initialization phase with a duration of 2 h. In this study we are only referring to results for visible clouds (i.e., nonzero LWC) in the cloud layer.

The mean vertical profiles of potential temperature and total water mixing ratio in the simulations, averaged over the horizontal domain and the simulation period, are shown in Fig. 2. The results show a well-mixed layer with a depth of about 500 m and an inversion above about 1500 m. The spread between the results of different models is largest in the inversion layer. The individual profiles are averaged in order to obtain vertical profiles for the applications of the parameterizations (Fig. 2). For this, the profiles of mean potential temperature and total water mixing ratio are provided on a grid with an increasing grid size with altitude. The grid size increases from $\Delta z = 48$ m near the surface to $\Delta z = 121$ m for the level centered at $z = 592$ m near the top of the boundary layer and to $\Delta z = 340$ m for the level centered at $z = 2186$ m. This resolution is close to that used in the third generation AGCM of the Canadian Centre for Climate Modelling and Analysis (CCCma), which uses a hybrid pressure-based vertical coordinate. The grid size is also typical of other such models.

The cloud base z_b is determined as that level at which the mass fluxes and cloud cover are at maximum in the LES results, which is at about $z = 600$ m. In the applications of the parameterization, $z_b = 606$ m is used, corresponding to the lifting condensation level (LCL) of a parcel that is lifted from the 5th level above ground at $z = 470$ m.

1) Calibration of subcloud vertical transport processes

The first issue that is addressed in the context of the LES results is how well cloud inhomogeneities and associated vertical fluxes can be represented by the parameterization. In particular, the goal is to find an approach for $p(f)$ that produces a reasonably close match between the values of α from the LES results and the parameterization. For this purpose, two profiles of α are calculated for the mean vertical fluxes of liquid water potential temperature θ_l and the total water mixing ratio r_t and from the mean vertical mass flux in the simulated LES cloud ensembles, using Eqs. (6) and (7). In the following, the versions DECORE and EQPROB of the parameterization, as described in section 3a, are applied and the results compared to the results of the LES models for α.

Figure 3 shows results for α from the LES models KNMI, MPI, NCAR, and UOK (thin lines). The results of the models UKMO and WVU are considerably different from those displayed in the figure. Additionally, the vertical profiles of $\overline{w\theta_l}^c$ and $\overline{wr_t}^c$ are considerably

[1] Available at http://www.knmi.nl/~siebesma/gcss/bomex.html.

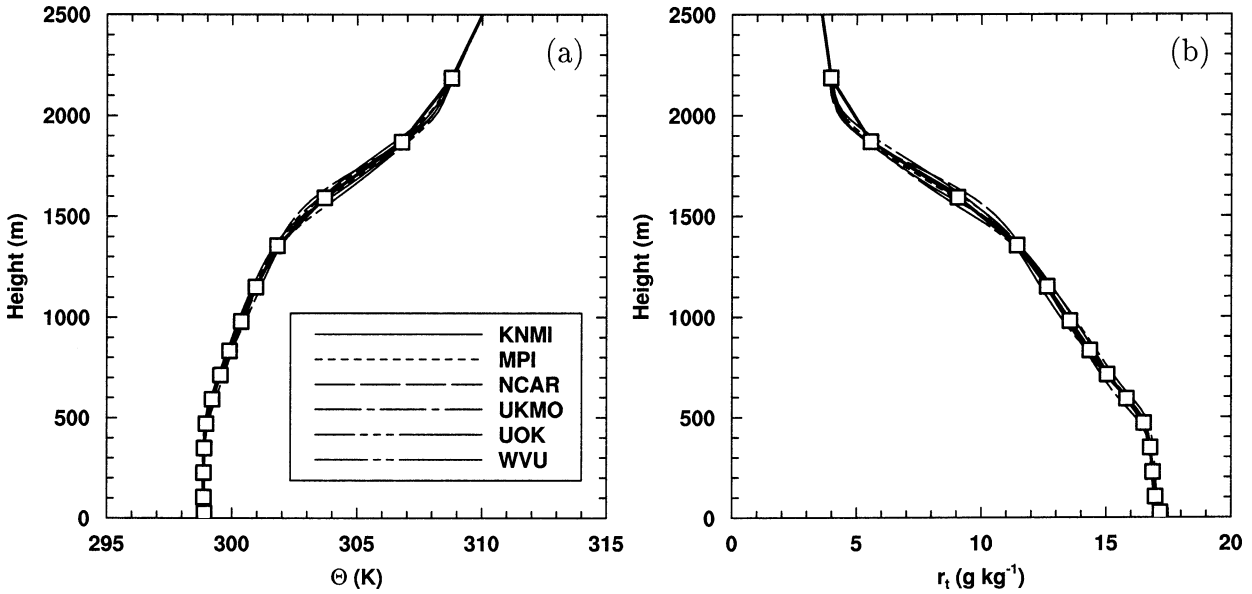

FIG. 2. Mean profiles of (a) potential temperature and (b) total water mixing ratio. The thin lines refer to the mean domain-averaged results of the 6 LES models according to the chart in (a) for a simulation period of 4 h. The squares and thick line refer to the average result for all LES models and the vertical grid used in the current simulations.

different from the corresponding fluxes of the other LES models. Consequently, the results of these models are not included in Fig. 3.

The small values of α obtained from the LES models near cloud base are consistent with top-hat distributed in-cloud properties at these levels. This suggests that downdrafts are not likely to penetrate to levels near cloud base. Above cloud base, α increases monotonically with height in all four simulations. Although the spread in the results also increases with height it is apparent that α has its maximum somewhere near the middle of the cloud layer. The cause of the scatter between the results of the individual models may at least in part be caused by different vertical velocities in the cloud ensembles in each simulation. The lowest values of w_c are simulated in the MPI model (results are later shown in Fig. 7). A lower value of w_c may be indicative for a stronger erosion of the cloud tops and hence larger

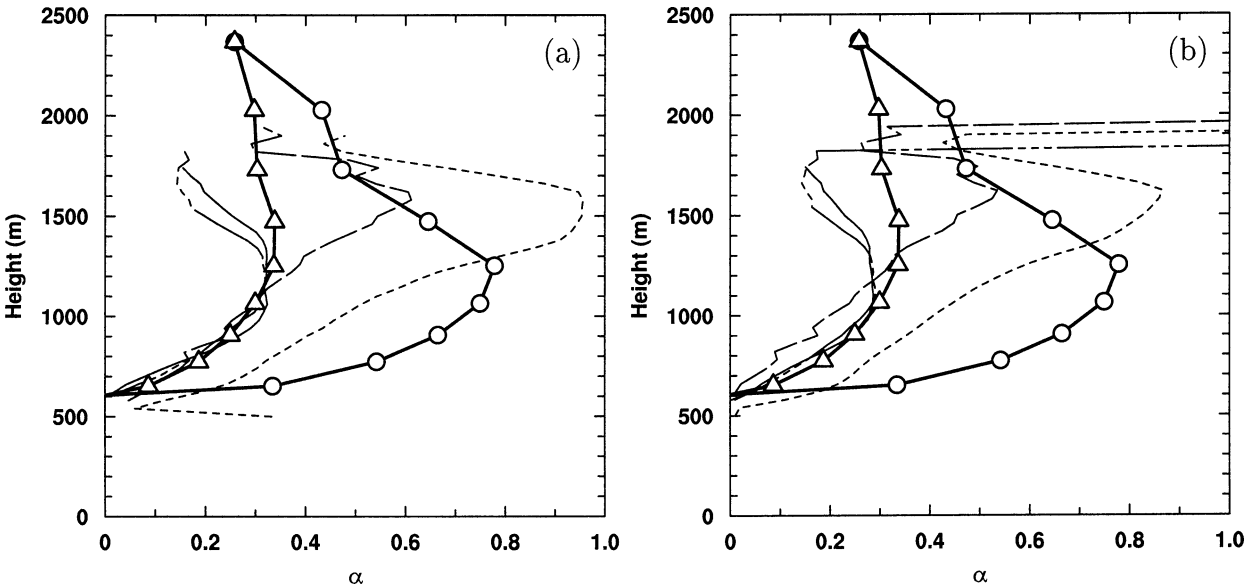

FIG. 3. Cloud-top entrainment parameter α for (a) liquid water potential temperature θ_l, (b) total water mixing ratio r_t for the results of the LES models KNMI, MPI, NCAR, and UOK (thin lines), according to the chart included in Fig. 2. Triangles refer to results of the version DECORE and circles to results of EQPROB of the parameterization as described in the text.

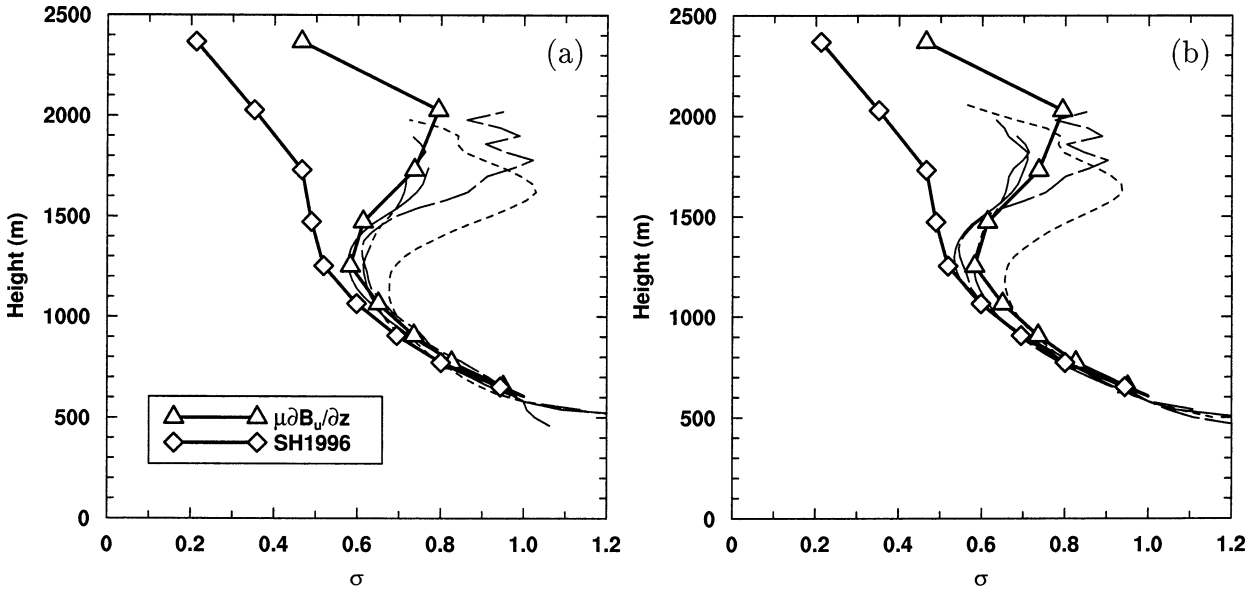

FIG. 4. Excess flux fractions σ for (a) liquid water potential temperature θ_l, (b) total water mixing ratio r_t for the results of the models KNMI, MPI, NCAR, and UOK (thin lines), according to the chart included in Fig. 2. Triangles refer to results of simulation DECORE in which the organized lateral mixing is parameterized in terms of the vertical gradient of buoyancy. Diamonds refer to the results of SH1996.

values of α. This appears to be likely since the ascending cloud tops are longer exposed to mixing processes if the cloud top ascends slowly. Differences in the results near the base and the top of the cloud layer may also be caused by too short sampling times since the results at these levels are dominated by sporadic events.

Results of the parameterization in Fig. 3 are shown for version DECORE of the parameterization for $\varphi = 1 \times 10^{-3}$ s^{-1}. There is good agreement between the results of the LES models and DECORE, especially near cloud base with this particular fit of φ to the data. Results near the inversion are highly uncertain due to large differences between the results of the LES models. In contrast, EQPROB tends to overestimate the cloud inhomogeneities throughout the cloud layer.

The results of EQPROB, DECORE, and TOPHAT (i.e., $\alpha = 0$) cover roughly the range of uncertainty for α. Therefore, results of these versions of the parameterization can be used to estimate the sensitivity of the approach to this parameter.

2) CALIBRATION OF ORGANIZED LATERAL MIXING

Since there is no standard method to distinguish organized lateral entrainment from other entrainment processes in LES simulations or field observations, the excess flux fraction σ is introduced, which is defined at each level above cloud base by

$$\sigma w_c \chi_b + (1 - \sigma) w_c \chi_e \equiv \overline{w\chi}^c, \tag{30}$$

or with the notation introduced above:

$$\sigma = \frac{\tilde{\chi} - \chi_e}{\chi_b - \chi_e}, \tag{31}$$

with $\tilde{\chi}$ given by Eq. (9), χ_b the value of the cloud property at cloud base, and χ_e the value in the cloud environment.

For top-hat distributed and conserved cloud properties, σ represents a unique measure of the degree of dilution by organized lateral mixing processes above cloud base. For all other distributions, σ can only be uniquely related to the efficiency of the organized lateral mixing if $d = 0$ according to Eq. (28). It can also be shown that σ has the same value for all conserved in-cloud properties that fall along a single mixing line. Further, σ is unity if no organized lateral entrainment or detrainment occurs; that is, $e = d = 0$. It can be easily shown that σ equally measures the efficiency of organized lateral entrainment in the approach of SH1996 with $\tilde{\chi} \equiv \chi_c$ in that approach.

The application of Eq. (30) to the LES results and to the parameterizations leads to the vertical profiles of the excess flux fractions σ for liquid water potential temperature and total water mixing ratio shown in Fig. 4. The results for the models KNMI, MPI, NCAR, and UOK are very similar. Decreases of the values with height in the lower portion of the cloud layer correspond to reductions in $\tilde{\theta}_l$ and $\tilde{r}_t$. These reductions are attributed to dilution of the clouds by organized lateral entrainment. Above about $z = 1200$ m, increases in the values of σ in the upper portion of the cloud layers are mainly caused by changes in the environmental values and only relatively small changes in $\tilde{\theta}_l$ and $\tilde{r}_t$ with height. This is consistent with the assumption that organized lateral detrainment is of relatively low importance for these LES results.

The corresponding results of the models UKMO and

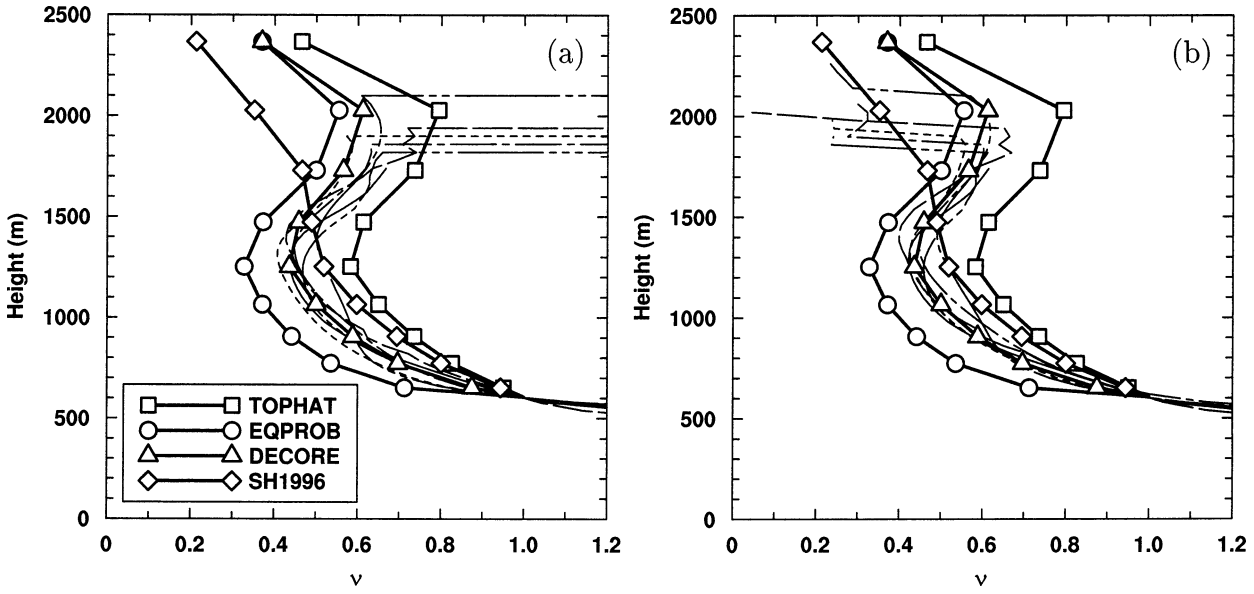

FIG. 5. Mixing fractions ν for (a) liquid water potential temperature θ_l, (b) total water mixing ratio r_t. Thin lines refer to LES model results according to Fig. 2. Squares refer to results of simulation TOPHAT, circles to EQPROB, triangles to DECORE, and diamonds to the results of SH1996.

WVU are in considerable disagreement with the other LES models. These results are not shown in Fig. 4.

Values of σ, calculated with Tiedtke's parameterization and the modifications suggested by SH1996, are in good agreement with the LES results near cloud base. However, the results give evidence for much too strong lateral entrainment in the upper portion of the cloud layer (Fig. 4). Additionally, the parameterization does not reproduce the characteristic minimum at about $z = 1200$ m.

In contrast to the results of Tiedtke's parameterization, the parameterization of organized lateral entrainment and detrainment in terms of buoyancy gradients according to Eq. (23) gives very good agreement with the LES results at all levels for a fit with $\mu = 14$ s^2 m^{-1} to the data. Organized lateral entrainment occurs below $z = 1473$ m, and organized lateral detrainment above this level in this application of the parameterizations. Hence results for σ in Fig. 4 above this level are dependent upon the values of α at these levels [cf. Eq. (28)]. However, owing to relatively small values of α at these levels, results with $d = 0$ are very similar to the results shown in Fig. 4.

3) COMPARISONS OF IN-CLOUD PROPERTIES AND FLUXES

With the values of μ and α given by calibration, the different versions of the parameterization can be tested with regard to a consistent representation of the mass fluxes and distributions of conserved properties in the simulated clouds.

In order to see how well the time-averaged mixing ratios of conserved properties in the cloud ensembles are represented, the LES results and the parameterizations are used to calculate the excess fractions,

$$\nu \equiv \frac{\chi_c - \chi_e}{\chi_b - \chi_e},$$

of the mixing ratios of θ_l and r_t in the ensembles. From Eq. (8) it follows that $\nu = (1 - f_c)\sigma$. Therefore, ν depends strongly on both the parameterization of organized lateral mixing and on the treatment of cloud inhomogeneities. For results of TOPHAT and SH1996's approach, $\nu = \sigma$. As discussed earlier, cloud-top entrainment is associated with values $f_c > 0$. Therefore, it generally has to be true that $\nu \leq \sigma$.

Results for all 6 LES models and for the parameterizations are displayed in Fig. 5. The vertical profiles are similar in shape to those in Fig. 4 but clearly have lower values at any level above cloud base. This means that inhomogeneities in the distributions of in-cloud properties cannot be neglected and that $w_c\chi_c < \overline{w\chi}^c$.

The overall best approximation to the LES results according to Fig. 4 is achieved by the results of version DECORE. The values are within in the range obtained from the LES results at all levels.

Excessive values of ν are computed in the version TOPHAT and in the approach of SH1996 near cloud base. As already apparent in the results for σ, SH1996's approach also leads to large differences in the profiles of the cloud-averaged values of θ_l and r_t in the upper portions of the cloud ensemble. These findings for SH1996 are generally consistent with the results of Raga et al. (1990). They applied a simple entraining plume approach with constant fractional entrainment rates to

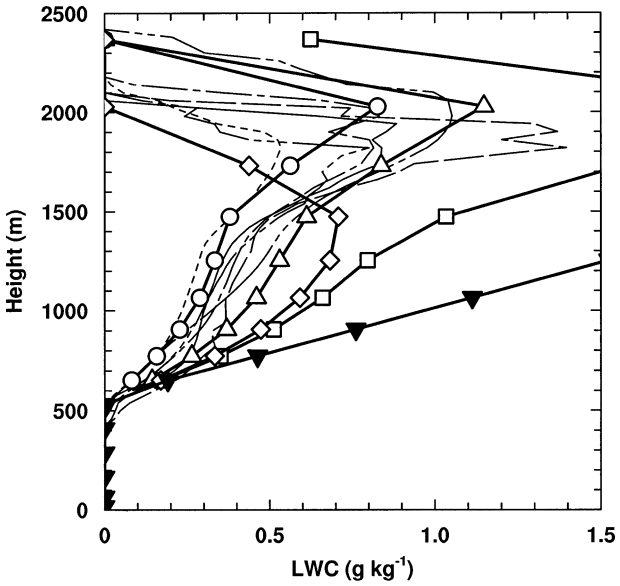

FIG. 6. Mean liquid water content in the clouds for results of the LES models and parameterizations according to Figs. 2 and 5. Solid downward pointing triangles refer to adiabatic values.

cloud bands observed off the coast of Hawaii, similar to the treatment of mixing in the approach of SH1996. Their results give evidence for good agreement between simulated and observed wet equivalent potential temperature and liquid water content near cloud base. However, the simulated values are considerably lower than observed in the upper portion of the cloud layer.

The LNB derived from the results shown in Fig. 5 is at $z_t = 1720$ m for DECORE, $z_t = 1552$ m for EQPROB, $z_t = 2229$ m for TOPHAT, and $z_t = 1593$ m for SH1996. As pointed out before, the diagnostic results for the LES models are not representative near the top of the cloud layer owing to low statistical significance and uncertainties in the interpolates. Although these results cannot be used in an interpretation they are included in the figure in an attempt to present the complete diagnostic dataset.

Results of EQPROB and DECORE for the mean liquid water content agree well with the LES results (Fig. 6). More vigorous mixing at cloud top in EQPROB compared to DECORE leads to lower liquid water mixing ratios in this version of the parameterization (cf. Fig. 3). Similar to the results of EQPROB and DECORE, LES models that produce larger values of α also tend to produce smaller liquid water contents (e.g., compare results of MPI and NCAR in Fig. 3 and Fig. 6). In contrast, the omission of cloud-top mixing processes in TOPHAT and SH1996 leads to overall much larger liquid water contents. Values produced by these parameterizations are in considerable disagreement with the results of the LES models near cloud base. However, in the upper portion of the cloud layer, SH1996 produces unrealistically low values. These results give support to the earlier notion that the assumption of a constant fractional entrainment rate in SH1996 is not very realistic. Additionally, results in Fig. 6 give clear evidence for the importance of cloud-top mixing processes for the treatment of liquid water contents in shallow cumuli.

Equation (29) is used to calculate the mean vertical velocities in DECORE, TOPHAT, and EQPROB. In the context of SH1996, w_c is diagnosed from

$$\frac{1}{2}\frac{\partial w_c^2}{\partial z} = \frac{B_c}{(1 + \gamma)} - \epsilon_u w_c^2,$$

above cloud base.

Generally, fluxes and cloud properties at the lower boundary of the cloud, such as the mean vertical velocity at cloud base, need to be determined through introduction of an additional closure assumption (Nitta 1975). As mentioned earlier, the relevant processes in the boundary layer that determine the magnitude of the vertical velocity at cloud base are not considered in the present study. Here $w_b = 0.3$ m s^{-1} is used as the lower boundary condition for w_c at $z = z_b$.

As discussed earlier, there is considerable uncertainty with regard to the magnitude of γ. As a first approach, $\gamma = 5$ is used in all parameterizations. This choice produces good agreement between most of the mean parameterized vertical velocities and mean results from the LES models near cloud base within the spread between the LES results (Fig. 7a), despite being much larger than the value typically used in one-dimensional cumulus models (Simpson and Wiggert 1969).

The large sensitivity of the mean vertical velocities to the value of γ is illustrated in Fig. 7. In Fig. 7a, $\gamma = 5$ is used in the applications of the parameterizations. Compared to the simulation with $\gamma = 0$ (Fig. 7b), the mean vertical velocities are typically smaller by more than 50% in the results of the parameterizations.

However, the parameterized vertical velocities in DECORE and EQPROB compare well to the mean LES results obtained for positively buoyant cloudy air for $\gamma = 0$ (Fig. 7b). A comparison of the LES results in Figs. 7a,b give evidence for large contributions of negatively or neutrally buoyant air to the mean vertical velocities in the simulated clouds. An analysis of LES results for the mean fractional area occupied by positively buoyant air in the cloud gives evidence that 55% to 75% of the air in the clouds is positively buoyant below $z = 1250$ m (not shown). In contrast, an integration of the probability density function over the positively buoyant region in the clouds simulated in DECORE yields that more than 97.5% of the air in the cloud is positively buoyant at all levels below $z = 1252$ m. Above that level, the fraction of positively buoyant air decreases monotonically with height to 63% at the top of the cloud layer.

One possible interpretation of the differences between the mean vertical velocities and the amounts of positively buoyant air in DECORE and the LES results appears to be that negatively and neutrally buoyant air

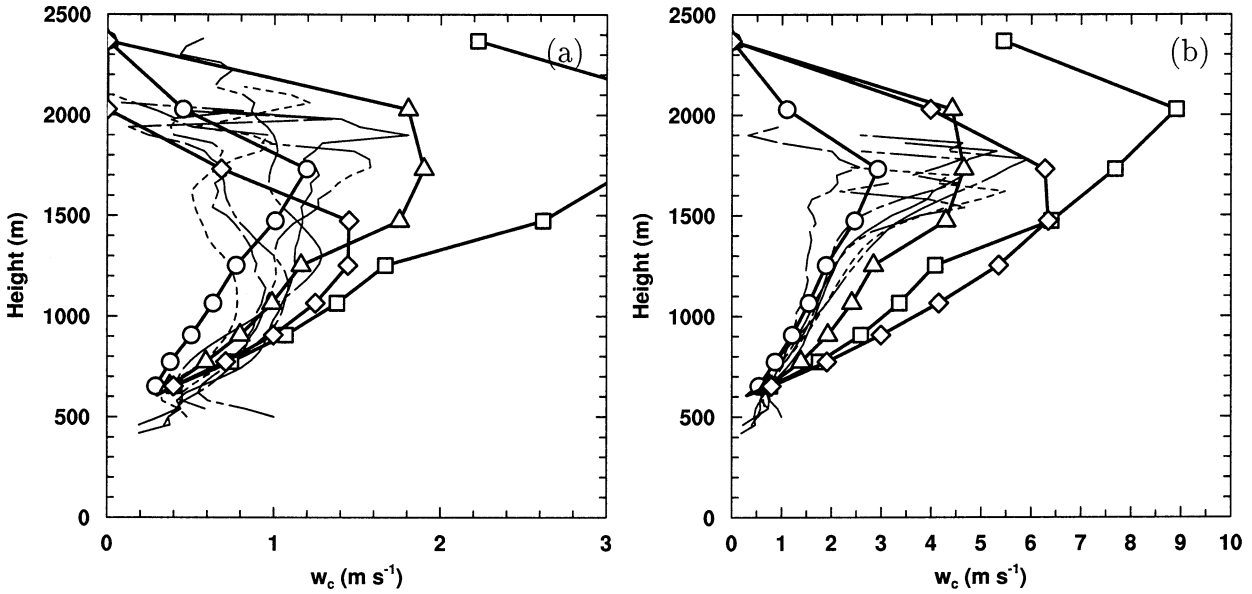

FIG. 7. Mean vertical velocities in the clouds for the results of the LES models and parameterizations according to Figs. 2 and 5. LES results in (a) refer to air with nonzero LWC and (b) to positively buoyant air with nonzero LWC. Results of the parameterizations are shown for the choices (a) $\gamma = 5$ and (b) $\gamma = 0$.

parcels are produced outside the active shallow cumulus clouds or during the final stage of the life cycle of the cumulus clouds in the LES simulations (see also the introduction and section 2). The mean vertical velocities associated with air parcels that occur after the growth phase of the cumulus life cycle ($t > \tau$) can be expected to be negative or at least much smaller than the vertical velocities shown in Fig. 7b. Owing to the large relative humidities in the LES simulations (e.g., between RH = 95% to 96% in a layer between $z = 450$ and 1000 m) these air parcels may remain saturated for a long time period relative to the cloud lifetime τ in DECORE, EQPROB, and TOPHAT. However, according to the simplified cloud life cycle in these parameterizations, effects of any saturated air parcels that exist after the collapse of the cloud at $t = \tau$ are omitted. Parameterization results shown in Fig. 7 only refer to mean vertical velocities within the cumulus clouds at $t \leq \tau$. Hence mean buoyancies and vertical velocities in the parameterized clouds may be large compared to the LES results in Fig. 7a. However, the good agreement with results for the mean cloud properties (Fig. 5) and LWC (Fig. 6) suggests that these important parameters are not strongly affected by processes occurring in the final stage of the cloud life cycles.

Unfortunately, there are no LES results available to directly test the importance of air parcels that exist in the later stages of the shallow cumulus life cycle. Therefore, the mean LES results can only be used to determine the range of γ in the parameterization that is consistent with the LES results.

Another interpretation of the differences in Fig. 7 is that drag and perturbation pressure gradients at the edges of the clouds may have considerable impacts on the vertical momentum budget and that these effects are not sufficiently accounted for.

Figure 8a shows the time-averaged fractional cloud cover $\langle a \rangle$, normalized by cloud base mass flux M_b. The normalization allows a direct comparison between results of the LES models and the parameterizations without the need to evaluate M_b. It is evident that the assumptions made in SH1996, DECORE, and TOPHAT lead to very accurate representations of the fractional cloud cover with the choice $\gamma = 5$. For $\gamma = 0$, substantially lower cloud amounts are calculated in DECORE (Fig. 8b). This figure also includes results of a simulation with DECORE in which cloud-top detrainment is included with $D_i = E_i$ (section 2d), showing that the cloud amount is not very sensitive to the treatment of cloud-top detrainment.

Relatively large differences exist between the results of the LES models for the mean vertical mass fluxes normalized by M_b (Fig. 9). The results of EQPROB and DECORE are well within the range of the predicted values from the LES results. Large differences occur for TOPHAT owing to a large vertical extent of the clouds simulated with this version of the parameterization. A major difference between SH1996 and the other results is that the vertical mass flux drops from a relatively large value at cloud top to zero directly above the cloud top in this parameterization whereas the other profiles are smooth near cloud top. The discontinuity can be attributed to the omission of life cycle effects in SH1996's approach. The assumption of a time-dependent fractional cloud cover results in more realistic profiles near the top of the cloud layer.

The mean vertical mass flux calculated in DECORE

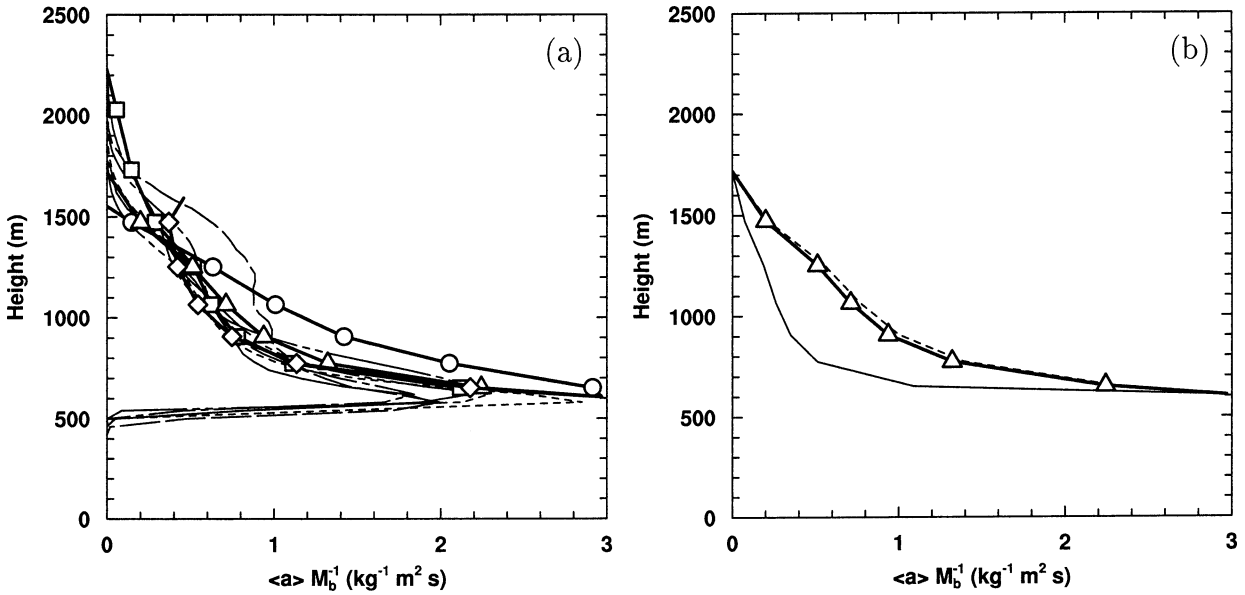

FIG. 8. Mean profiles of the normalized fractional cloud cover (a) for the results of the LES models and parameterizations according to Figs. 2 and 5. Results in (b) refer to DECORE for $\gamma = 5$ and without cloud-top detrainment (triangles), $\gamma = 0$ and without cloud-top detrainment (thin full line), and for $\gamma = 5$ and with cloud-top detrainment (thin dotted line).

is insensitive to the value of γ (Fig. 9b). Only slightly smaller vertical mass fluxes are obtained with $\gamma = 0$ compared to the reference simulation with $\gamma = 5$. The reason for the low sensitivity is that t_* and τ scale in a similar way with γ. Hence M_c is insensitive to differences in t_* and τ (see section 2). Similar to the cloud amount, the introduction of cloud-top detrainment does not lead to considerably different values of M_c (Fig. 9b).

With regard to the effects of shallow clouds on the large-scale environment, it is also desirable to compare the entrainment and detrainment fluxes in the cloud ensembles that are inherent in the results of the parameterizations and LES models. Unfortunately, there is no straightforward approach to obtain these fluxes from LES results and a few assumptions are necessary in order to arrive at meaningful estimates. Probably the most obvious choice is to derive the entrainment and detrainment fluxes from averaged continuity equations

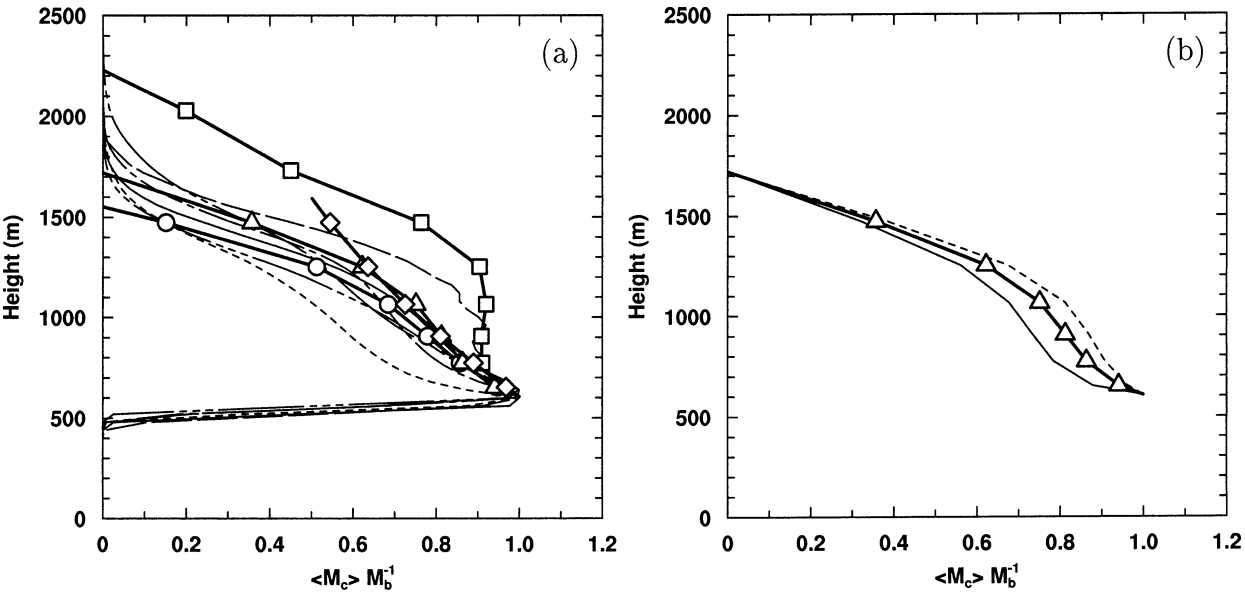

FIG. 9. Mean profiles of the normalized vertical mass flux (a) for the results of the LES models and parameterizations according to Figs. 2 and 5. Results in (b) refer to DECORE for $\gamma = 5$ and without cloud-top detrainment (triangles), $\gamma = 0$ and without cloud-top detrainment (thin full line), and for $\gamma = 5$ and with cloud-top detrainment (thin dotted line).

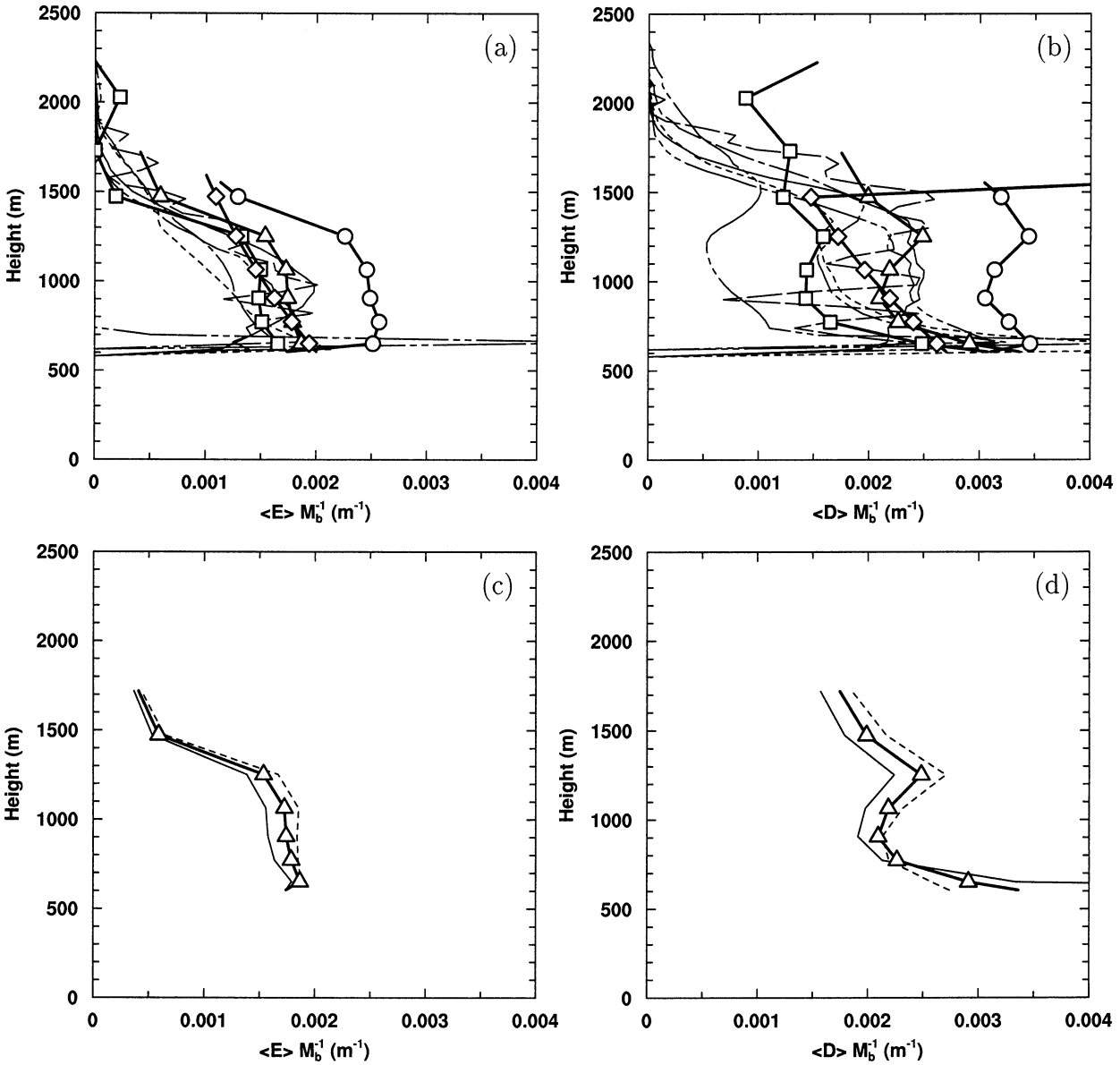

FIG. 10. Mean profiles of normalized (a) entrainment and (b) detrainment mass fluxes for the results of the LES models and parameterizations according to Figs. 2 and 5. Normalized (c) entrainment and (d) detrainment for DECORE for $\gamma = 5$ and without cloud-top detrainment (triangles), $\gamma = 0$ and without cloud-top detrainment (thin full line), and for $\gamma = 5$ and with cloud-top detrainment (thin dotted line).

under the assumption that the large-scale meteorological situation and the cloud ensemble properties are sufficiently steady. Further suppose that the source level for the entrained air is near the local level of entrainment and that the detrained air has characteristics that are very similar to the horizontally averaged cloud air properties at that level. Consequently, the continuity equations for θ_l and r_t can be written as

$$\langle E\rangle\theta_{le} - \langle D\rangle\theta_{lc} - \frac{\partial}{\partial z}(\rho\langle a\rangle\overline{w\theta_l}^c) = 0, \qquad (32)$$

$$\langle E\rangle r_{te} - \langle D\rangle r_{lc} - \frac{\partial}{\partial z}(\rho\langle a\rangle\overline{wr_t}^c) = 0, \qquad (33)$$

where $\langle E\rangle$ and $\langle D\rangle$ refer to all entrainment and detrainment processes, including contributions of D_f.

Equations (32) and (33) can be directly applied to the LES results in order to determine $\langle E\rangle M_b^{-1}$ and $\langle D\rangle M_b^{-1}$. The resulting fluxes in Figs. 10a,b agree well with previously published results for the same case (Siebesma and Cuijpers 1995). However, the spread in the results is considerable and it appears that in particular the results of the models WVU and UKMO differ from the results of the other models. These differences are consistent with the differences described earlier (Figs. 3 and 4).

Results of the approaches DECORE and TOPHAT in

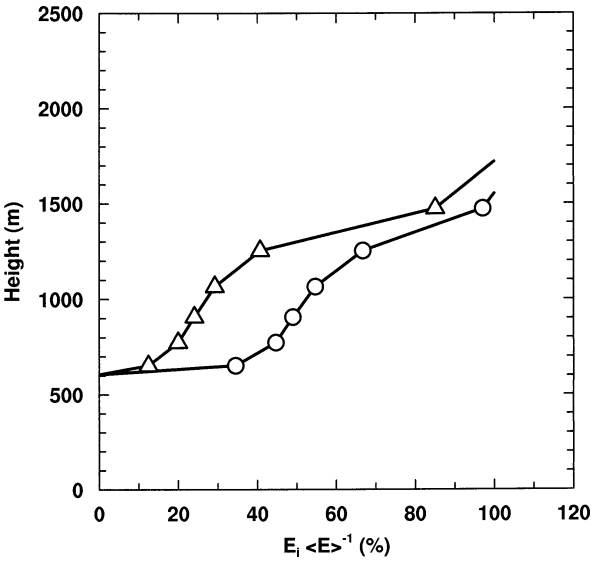

FIG. 11. Relative contributions of cloud-top entrainment to the total entrainment mass fluxes in the cloud ensembles for DECORE (triangles) and EQPROB (circles).

Figs. 10a,b are generally in good agreement with the LES entrainment fluxes. The overall best agreement is found for version DECORE. EQPROB produces excessive entrainment and detrainment fluxes.

A striking feature of the diagnosed detrainment flux for SH1996's parameterization is that a large fraction of the detrainment is confined to a narrow layer near the top of the cloud. This characteristic feature becomes even more evident at higher vertical grid resolution. The reason for this is that the detrainment at the top of the cloud layer is a delta function in this approach that is determined by the magnitude of the vertical mass flux at cloud top.

Similar to the results shown in Fig. 9, the entrainment and detrainment fluxes in DECORE are not very sensitive to the value of γ (Fig. 10c) and the formulation of cloud-top detrainment (Fig. 10d).

The relative contribution of the cloud-top entrainment fluxes E_i to the time-averaged ensemble-mean entrainment mass flux, $\langle E \rangle$ is shown in Fig. 11. According to the results for parameterization versions EQPROB and DECORE, the contribution of cloud-top entrainment is negligible near cloud base. In contrast, cloud-top entrainment is the predominant entrainment process in the upper portion of the cloud layer. At cloud top, the dilution of the cloud occurs exclusively by cloud-top entrainment. Organized lateral entrainment does not contribute to the total entrainment because the vertical gradient of the undiluted parcel buoyancy is negative near cloud top.

If accounted for, the contribution of cloud-top detrainment to the total detrainment is much smaller than the contribution of final detrainment. Less than 26% of the total detrainment is associated with D_i in the simulation with DECORE and $D_i = E_i$ (Figs. 8 to 10).

d. Large-scale heat and moisture budgets in BOMEX

In this section, the parameterization is applied to the mean observed meteorological situation in the BOMEX domain. The results are compared with the analyses of large-scale heat and moisture budgets of Nitta and Esbensen (1974).

Only results for 22 and 23 June are considered since the fluxes during these days are very similar whereas the situation changes considerably on 24 June (Soong and Ogura 1976). The quasi-steady character of the situation is illustrated by the mean vertical profiles of potential temperature and total water vapor mixing ratio in Fig. 12. The profiles shown in this figure refer to time- and station-averaged results of rawindsonde soundings that were taken 15 times per day at each of the four corner ships in the experiment. The measurements were checked for inconsistencies and daytime humidity errors due to radiative heating of the hygristor elements of the rawindsondes were additionally corrected (Nitta and Esbensen 1974). There is good agreement between the measurements and the results of the LES models for the total water mixing ratios. However, the temperature is about 1 to 2 K lower in the lower part of the LES simulation domain, which is associated with slightly lower potential temperatures in the LES results (Fig. 12a).

Nitta and Esbensen (1974) used the corrected rawindsonde datasets to calculate the apparent heat source Q_1 and apparent moisture sink Q_2 (Yanai et al. 1973; Ogura and Cho 1973; Nitta 1975) for each day in the experiment. These quantities are obtained from the equations of the first law of thermodynamics and moisture continuity and can be written

$$Q_1 \equiv \frac{\partial \overline{s}}{\partial t} + \overline{\mathbf{V}} \cdot \nabla \overline{s} + w \frac{\partial \overline{s}}{\partial z},$$

$$Q_2 \equiv -L_v \left(\frac{\partial \overline{r}}{\partial t} + \overline{\mathbf{V}} \cdot \nabla \overline{r} + w \frac{\partial \overline{r}}{\partial z} \right),$$

where $s = c_p T + gz$ is the dry static energy, $\mathbf{V}$ the vector of the horizontal wind field, and w the vertical component of the wind. The overbars denote large-scale averages over a unit horizontal area. Q_1 includes the effects of heating and cooling due to radiation Q_R, condensation, evaporation, and eddy vertical transports of sensible heat caused by cumulus convection and turbulent motion. Accordingly, Q_2 refers to moisture sources and sinks due to condensation, evaporation, and eddy vertical transports. The quantities $Q_1 - Q_R$ and Q_2 can directly be used to determine the effects of cumulus clouds on the large-scale environment. The first part of this section focuses on results for $Q_1 - Q_R$ only and results for Q_2 will be shown at the end of this section.

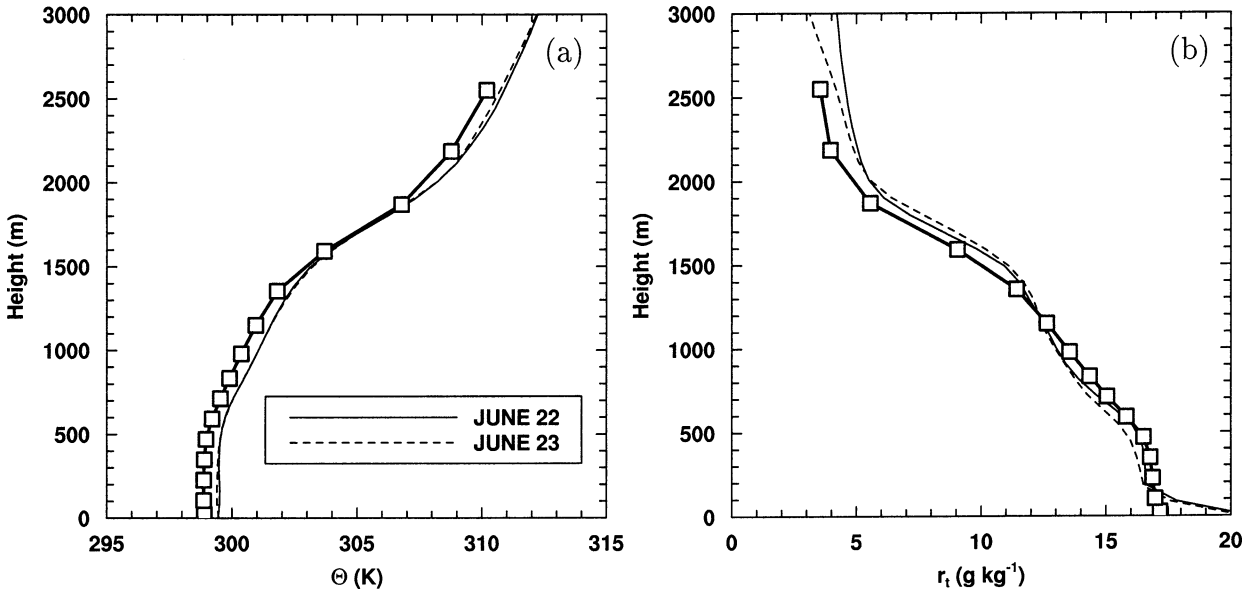

FIG. 12. Mean profiles of (a) potential temperature and (b) total water mixing ratio for 22 and 23 Jun 1969 during BOMEX from observations at the four corners of the experimental domain (Nitta and Esbensen 1974). Also shown are the mean results of the LES models used in Figs. 2 to 12 (thick line and squares) for comparison.

In the applications of the parameterizations, a grid with a vertical grid size of 10 hPa is used. The cloud-base mass flux is prescribed to $M_b = 288$ hPa day^{-1} according to the value obtained by Nitta (1975) for the period 22 to 24 June in BOMEX. The parameterizations are separately applied to each day but only the mean results for the period 22 to 23 June are used in the comparisons.

In contrast to the comparison with the LES results in the previous section, it is not possible to directly obtain z_b from the analysis results. In order to address the uncertainties in z_b and cloud-base properties, the properties of the air at cloud base are estimated for the undiluted ascent of air parcels that are launched at different levels between 1 and 9 hPa above the sea surface at each day. The vertical distance between the launching levels is 1 hPa.

Mean vertical profiles of $Q_1 - Q_R$ for 22 and 23 June are shown in Fig. 13 using a given profile of Q_R (Holland and Rasmusson 1973). The results of Nitta and Esbensen (1974) give evidence for a maximum of the large-scale cooling slightly below $z = 2000$ m with a value of about 5 K day^{-1}. According to Nitta and Esbensen (1974), this maximum can be attributed to reevaporation of cloud droplets that detrain near the top of the trade inversion. The small values above about $z = 2300$ m indicate that there are very few clouds that penetrate into the layers above the inversion. Positive values in the layer from about $z = 600$ m to about $z = 1400$ m may be caused by adiabatic warming due to compensating downward motion in the cumulus environment. Below about $z = 600$ m, positive values are caused by turbulent motions of clear air in the mixed layer that are not considered in the parameterizations. Hence the following discussion refers to the layer above $z = 600$ m only.

All parameterizations introduced in the previous sections consistently produce much too low cloud tops even for air parcels launched very close to the surface (Fig. 13). The deepest cloud layers are produced in TOPHAT. But even in this simulation, the cloud tops are below about $z = 1800$ m, which is much lower than the representative cloud top according to the profiles of analyzed apparent heat source and moisture sink.

In order to achieve some understanding of the considerable disagreement between the parameterizations and the BOMEX analyses it is useful to note that the cloud tops of the bulk of the clouds in the cloud ensembles appear to be below $z = 1800$ m in all LES model results according to Figs. 9 and 10. This is much lower than the corresponding heights according to the analysis results in Fig. 13. This conclusion is consistent with the results of Siebesma and Cuijpers (1995) who obtain maximum cooling rates at about $z = 1600$ m in simulations with the KNMI model for BOMEX. Their results show substantial underestimations in the magnitudes of Q_1 and Q_2 above this level and slight overpredictions below. From the calibration of μ and α in the parameterization based on the LES results, it follows that biases in the predicted fluxes in the LES models are inherited by the parameterization through the calibration process.

It appears that the differences in the large-scale temperatures in the LES model simulations and in the analysis of Nitta and Esbensen do not explain the low cloud tops in the LES simulations (Fig. 12). In contrast, the lower temperature in the mean LES results and asso-

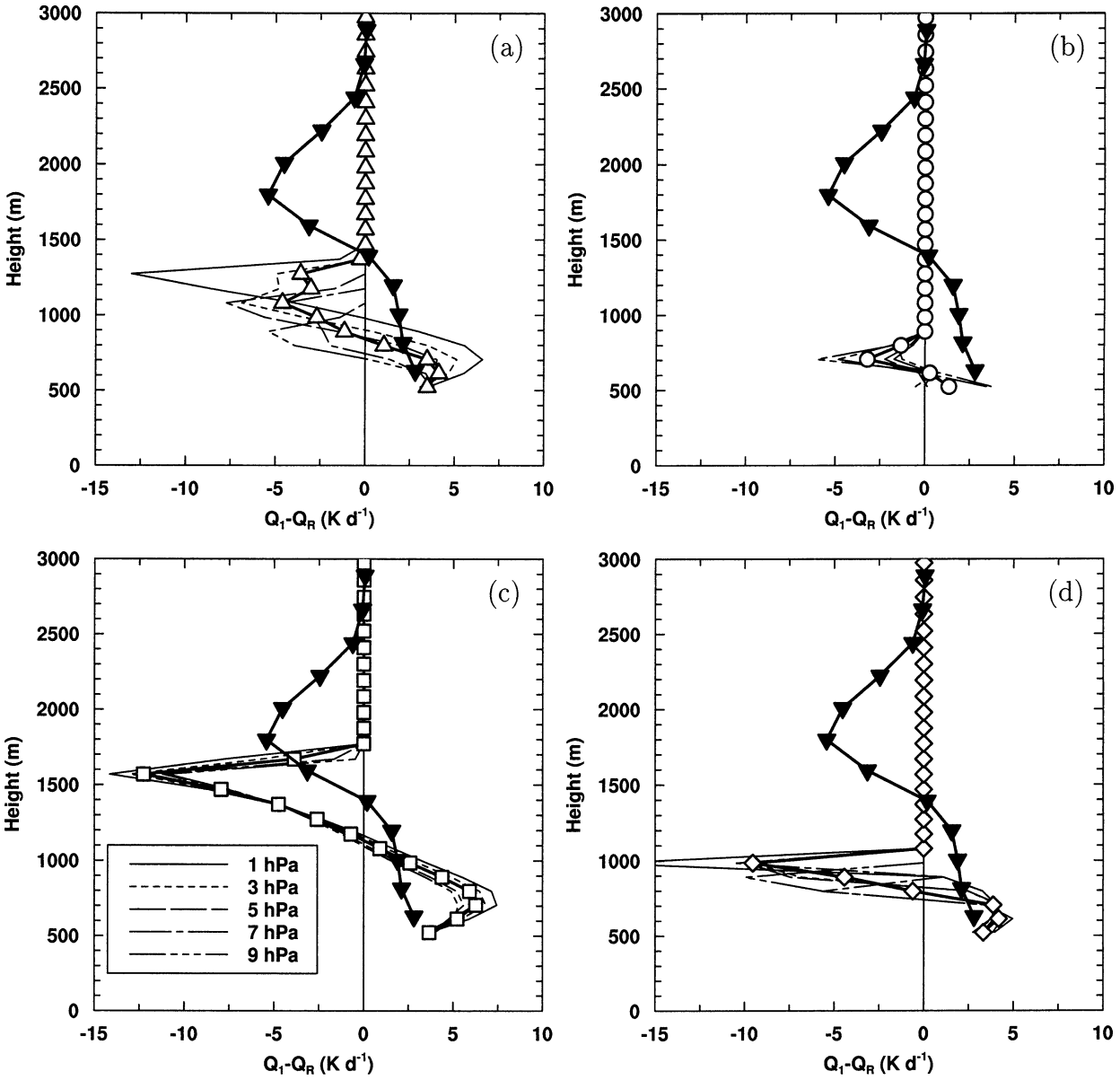

FIG. 13. Differences between apparent heat source and radiational heating for 22 to 23 Jun in simulations (a) DECORE, (b) EQPROB, (c) TOPHAT, and (d) for the results of SH1996. The thick line and solid downward pointing triangles refer to the results of Nitta and Esbensen (1974) during this period. Thin lines refer to the results for different launching levels of the initiating parcel of air. The height of these levels in hPa above sea level is given in the chart in (c). Averages of the simulation results at the different parcel launching levels over the 2-day period are marked by thick lines and symbols in (a) to (d). Only results above $z = 500$ m are shown.

ciated higher relative humidities most likely tend to produce too high tops in the LES models rather than too low cloud tops compared to the BOMEX observations. This conclusion is supported by results of sensitivity studies using the parameterization described in the previous sections for different large-scale temperature profiles. According to the results of the sensitivity studies, the height of the cloud tops is typically reduced by up to a few hundred meters if the large-scale temperature is increased by 2 K in simulations with the parameterizations if the total water mixing ratio is kept constant. The differences in the prescribed large-scale values of temperature explain to a large extend the differences between the results of the parameterizations in Fig. 13 and results presented in the previous sections.

While it is not clear from the results available in this study what causes the low cloud depths in the LES results for BOMEX, it needs to be emphasized here that entrainment processes simulated in LES models may be sensitive to the parameterizations of subgrid-scale processes in these models, to the conditions at the boundaries of the model domain, and to the numerical ap-

TABLE 1. Parameters of the numerical experiments.

Simulation	μ (s^2 m^{-1})	φ (s^{-1})
TOPHAT_A	6.0	0
DECORE_A	0	1×10^{-3}
DECORE_B	4.5	4×10^{-4}
EQPROB_A	0	∞

proaches. For example, results of a different LES model intercomparison project of the GCSS Boundary Layer Cloud working group give evidence that LES models tend to produce much too large entrainment rates if the variabilities in height and thickness of strong stratocumulus inversions are not adequately resolved by the model grid (Bretherton et al. 1999; Stevens and Bretherton 1999). Additionally, Brown (1999) found a strong sensitivity of the sizes of individual shallow clouds in LES model simulations for BOMEX but also an encouraging low sensitivity of ensemble-averaged statistics to grid sizes.

Since it is not possible to determine the causes for the discrepancies in Fig. 13 due to the lack of data on the properties of the clouds in BOMEX, an alternative is to recalibrate the parameterization by finding new values of the free parameters in the parameterization that lead to better agreement between the large-scale budgets. The approach pursued here is simply to match the levels at which the maxima in the heating and moistening profiles occur in the analysis results in order to obtain first approximations. This approach is not completely different from the approaches in other studies of the large-scale heat and moisture budgets in BOMEX (e.g., Soong and Ogura 1976).

Results of different parameterizations with new calibrations are shown for the apparent heat source (Fig. 14) and the apparent moisture sink (Fig. 15). The parameters used in the simulations are summarized in Table 1. Results of the version DECORE_A in Figs. 14a and 15a refer to simulations without any organized lateral entrainment or detrainment but otherwise with the same treatment of cloud-top entrainment as in DECORE. TOPHAT_A in Figs. 14b and 15b does not include any cloud inhomogeneities. The organized lateral mixing in TOPHAT_A is relatively weak compared to DECORE. DECORE_B in Figs. 14c and 15c includes cloud-top entrainment and organized lateral mixing. The magnitude of the entrainment and detrainment fluxes is small compared to DECORE. Finally, Figs. 14d and 15d show results of EQPROB_A for a parameterization that uses the same treatment of cloud inhomogeneities as in EQPROB but that does not include any organized lateral mixing.

For DECORE_A, excessive cooling is diagnosed at heights below about $z = 1500$ m and insufficient cooling above this level (Fig. 14a). Only results for parcels launched at the levels between 5 and 9 hPa are shown for DECORE_A. Parcels launched at the first two levels produce clouds that overshoot the inversion and cannot be considered as part of a shallow cumulus ensemble.

Very good agreement between analyzed and mean simulated heating rates are obtained for TOPHAT_A (Fig. 14b). Compared to the results of DECORE_A, TOPHAT_A produces very different cloud-top heights for different parcel launching levels. The mean results above about $z = 2000$ m are strongly affected by the results for the first parcel launching level above ground.

The approach used to determine φ and μ in DECORE_B is to fit the results of DECORE_B to DECORE with respect to the relative contributions of cloud-top entrainment to the total entrainment at all levels in the clouds. Hence the relative magnitudes of cloud-top and organized lateral entrainment are similar in DECORE_B and DECORE. The results of this procedure are shown in Fig. 16.

Good general agreement with the analysis is found for the results of DECORE_B (Fig. 14c). The results for each parcel launching level are similar to those for slightly higher parcel launching levels in TOPHAT_A (e.g., compare results for 1 hPa in DECORE_B to 3 hPa in TOPHAT_A). It appears that parcels lifted from 1 hPa produce the best agreement with the observations.

The results of EQPROB_A give evidence that the assumption of equal probabilities for the air mixtures in the cloud generally produces too low cloud tops (Fig. 14d). The results of this parameterization are similar to those of DECORE_A. These results suggest that cloud-top entrainment, without additional consideration of organized lateral entrainment, tends to produce excessive cooling near the bottom of the cloud layer and deficits near the trade inversion.

Differences between the results of the parameterization and the analysis may in part be attributable to variability in the large-scale thermodynamic profiles which are not accounted for in the parameterization. Also, uncertainties associated with M_B may affect the magnitudes of $Q_1 - Q_R$ and Q_2. However, the magnitude of M_B does not effect the relative magnitudes of the results shown in Figs. 13 to 15 [from Eq. (24)].

Finally, results for the apparent moisture sink shown in Fig. 15 are consistent with the results in Fig. 14 in the upper portion of the cloud layer. However, systematic overpredictions occur for the moistening rates in a layer that is centered at about $z = 1100$ m for all parameterizations. Although this discrepancy may indicate problems in the approaches it is interesting to note that the results of Soong and Ogura (1976), which are derived using a time-dependent, two-dimensional, axisymmetric cloud model, also show a similar minimum in Q_2 at about the same height for the same BOMEX period. Soong and Ogura (1976) speculate that the local maximum at this height in Nitta and Esbensen's data may be caused by the correction method they use for the humidity data. Also, Holland and Rasmusson (1973) report different results for Q_2 that they obtain with a different correction method. In particular, Holland and Rasmusson (1973) also find a local minimum in Q_2 at about the same height.

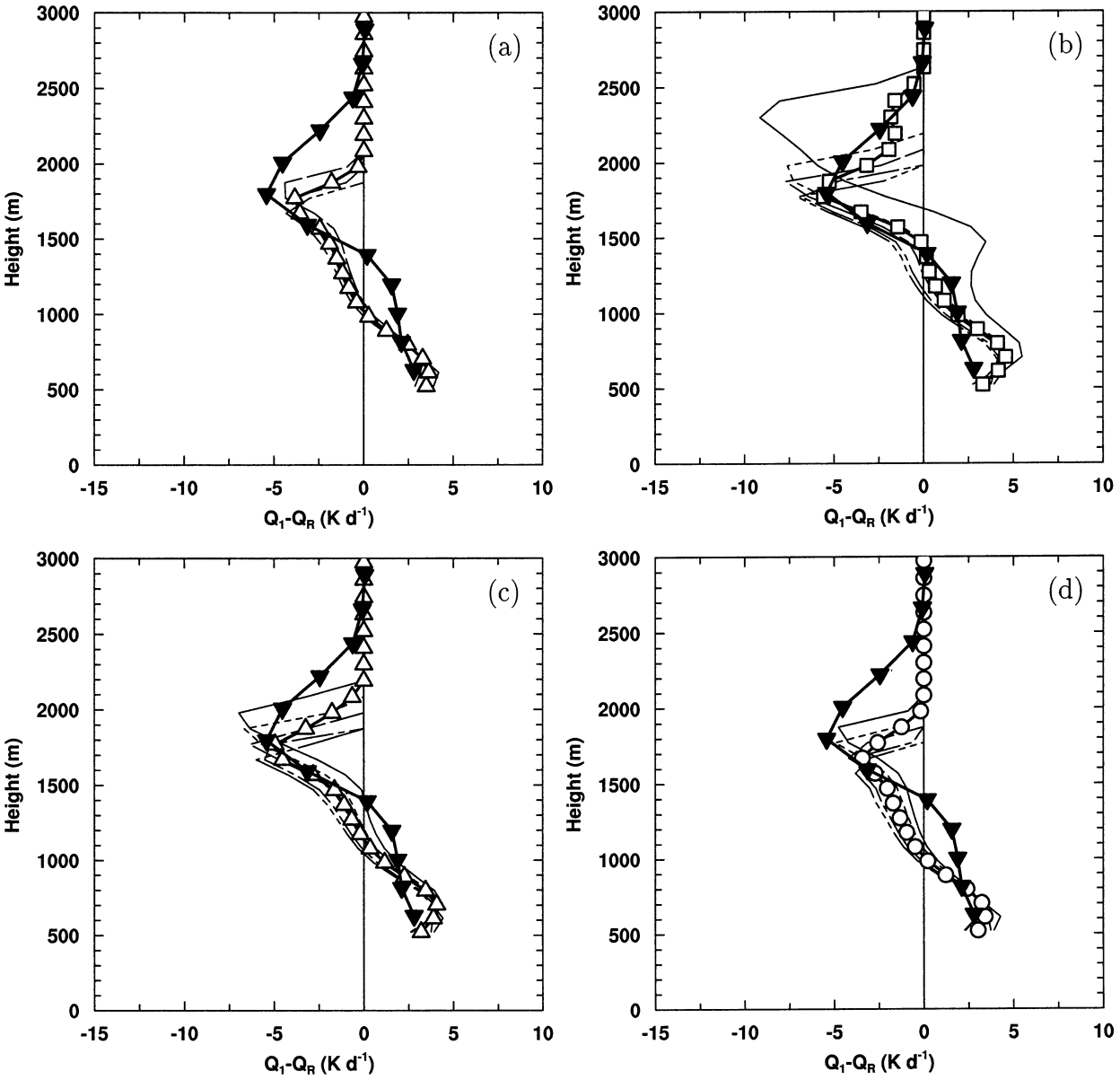

FIG. 14. As in Fig. 13, after refitting, for simulations (a) DECORE_A, (b) TOPHAT_A, (c) DECORE_B, and (d) EQPROB_A according to the text.

4. Discussion and conclusions

A new parameterization of the bulk effects of transient shallow cumulus clouds is proposed. In the parameterization, the physical properties of rising air parcels are modified by entrainment of environmental air into the ascending top of the cloud and also by organized entrainment at the lateral boundaries of the cloud. The cloud-top mixing is associated with horizontal inhomogeneities in the properties and fluxes in the cloud. Different physical hypotheses are introduced in order to obtain simple representations for the effects of cloud inhomogeneities in the parameterization. Finally, the initial growth phase of the cloud in the parameterization is terminated by an abrupt and complete collapse of the cloud during which the air remaining in the cloud is detrained into the environment. Based on these assumptions, budget equations for the vertical mass flux, conserved cloud properties, and vertical velocity are derived in order to represent the mean effects of a shallow cumulus clouds averaged over their life cycles.

The new parameterization is applied to observations and LES results from the undisturbed period in BOMEX from 22 to 23 June 1969. Application of the parameterization to LES results for this period produce consistent profiles of mean fluxes and properties in the cloud ensembles for version DECORE of the parameteriza-

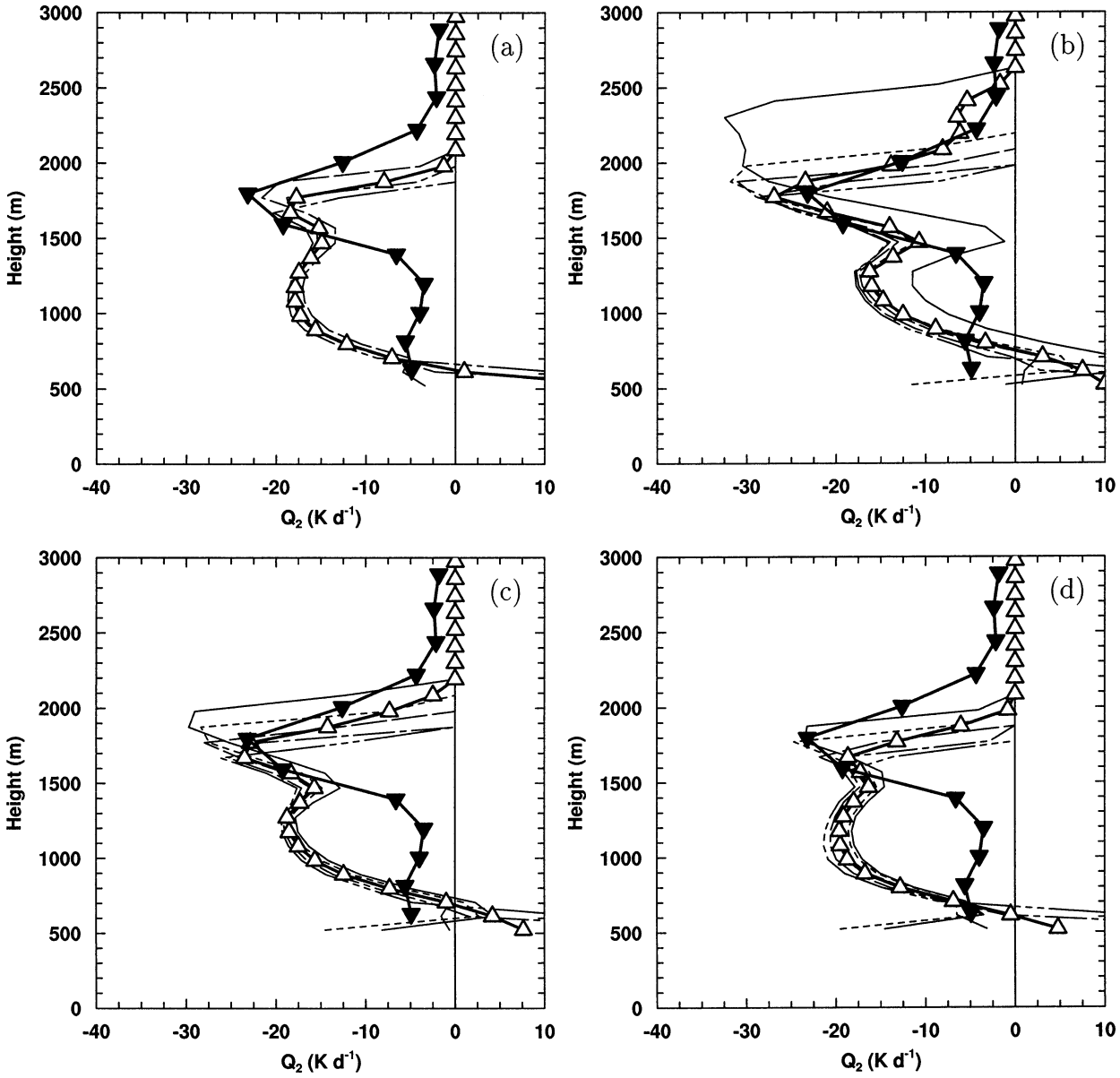

FIG. 15. As in Fig. 14, for the apparent moisture sink.

tion. It is found that entrainment at ascending cloud tops is the largest contribution to the total entrainment flux near the trade inversion in the LES simulations for BOMEX. Additionally, the results show that penetrative downdrafts do not affect the in-cloud properties and fluxes near the base of the clouds in the simulations.

Including the simple life cycle approach in the parameterization produces good agreement with LES results with respect to fluxes and properties near the top of the cloud layer. The contribution of the final detrainment flux near the end of the cloud life cycle is by far the largest contribution to the total detrainment flux. In contrast, the contribution of cloud-top detrainment is negligible.

Additional tests of large-scale heat and moisture budgets for the same period in BOMEX using results of an analysis by Nitta and Esbensen (1974) are also encouraging. It is shown that the proposed parameterization produces realistic cooling and moistening profiles below the inversion. However, these comparisons give no conclusive evidence regarding the nature of the entrainment process although it appears that mixing by organized lateral entrainment is important for the large-scale budgets. There is also evidence that the entrainment processes in observed clouds in BOMEX are less efficient than suggested by the LES results.

As noted in section 2 above, the effects of buoyancy sorting are ignored in the parameterization proposed

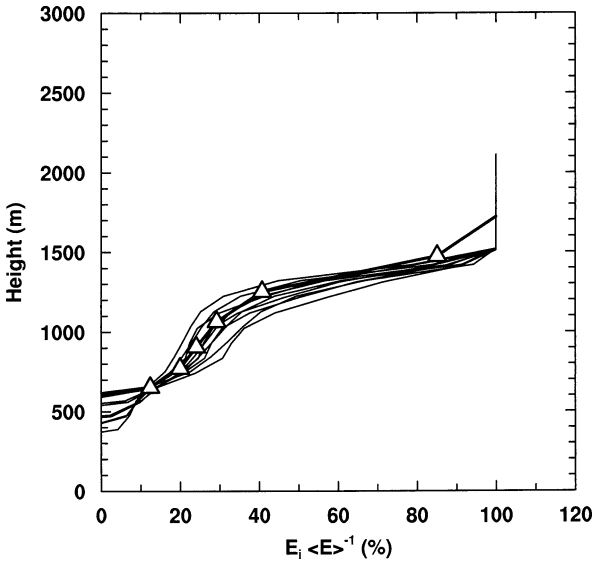

FIG. 16. Relative contributions of cloud-top entrainment to the total entrainment in simulation DECORE (thick line and triangles) and in DECORE_B for all days and parcel launching levels.

herein. Consequently certain aspects of the parameterization of large-scale heating and moistening effects are qualitatively different from current parameterizations based on the buoyancy sorting concept as applied to shallow cumulus regimes. An important difference is that in parameterizations based on the buoyancy sorting hypothesis the air, which is detrained into the environment, is nearly neutrally buoyant and free of liquid water (Emanuel 1991; Emanuel and Živković-Rothman 1999). A result of this is that detrainment will have a less important effect on the large-scale heat and moisture budgets than is the case in our parameterization. In particular, since the mean mass flux is always positive in our parameterization, all of the net cooling at top of the cloud layer is accomplished through evaporation of detrained liquid water. For the buoyancy sorting parameterizations this cooling is achieved predominantly through the action of negatively buoyant downdrafts that arise as a result of the buoyancy sorting mechanism. Cho (1977) also assumed that air that is finally detrained by shallow convective clouds at the end of their life cycles is free of condensed water and has the same temperature as the environment. Consequently in applying his representation to the BOMEX data he determined that a net downward convective mass flux is required in the upward part of the convective layer to account for the net cooling in that region.

It is noteworthy that the LES models for the most part produce small but positive values of the net convective mass flux in the region just below the trade inversion. The parameterization proposed herein is in good agreement with the LES results. However, the LES models may also suffer from deficiencies that limit their ability to adequately represent the true behavior of negatively buoyant downdrafts that typically occur in reality in the upper part of the convective layer. Thus the absence of a net downward mass flux in that region in the LES simulations does not negate the importance of the net effects of buoyancy sorting in that region. However, despite this possible shortcoming we have demonstrated that the parameterization herein is capable of reproducing the observed large-scale heat and moisture budgets in shallow convective regimes with considerable fidelity.

This study is entirely based on the BOMEX case, which also has been used in many other studies on processes associated with shallow convection. The reason for the decision to use BOMEX results in the present study was motivated by the fact that the datasets for this experiment appear to be relatively detailed and well documented in comparison to other studies. However, further investigations are required in order to validate the parameterization under different conditions.

A major problem in this study is that the calibration and validation of the parameterization is relatively difficult owing to the fact that insufficient data with respect to natural shallow convection is available from observations and cloud resolving model simulations. For example, more detailed observations of liquid water contents and total water mixing ratios at different heights and at different stages of cloud life cycles would be very useful in future development and testing of parameterizations. The main problem regarding the parameterization of cloud-top entrainment processes in the current approach is that no data are available that can be used to directly determine the probability density distributions of the air mixtures in the ascending cloud tops. Although the present study and numerous other studies strongly suggest that inhomogeneities in the distributions of air mixtures are important features in shallow clouds there are still large uncertainties with regard to the treatment of cloud inhomogeneities in the context of a parameterization.

The parameterization described in this paper is currently being tested in the fourth generation AGCM of the CCCma in order to study the effects of shallow convection on simulations of the global distributions of heat, moisture, and sulfur compounds. Results of these applications and the treatment of cloud base mass fluxes (i.e., the cloud base closure) will be reported in a following paper.

Acknowledgments. We are grateful to two anonymous reviewers for their very helpful comments and to Steven Esbensen who provided BOMEX large-scale budgets and profiles of environmental meteorological parameters. Also, we wish to thank Pier Siebesma for giving us permission to use results of the GCSS Boundary Layer Cloud working group model intercomparison project for the BOMEX shallow cumulus study. Thanks are further due to our colleagues John Scinocca, Virginie Lorant, and Richard Harvey for comments and discussions.

This research was supported by the Meteorological

Service of Canada through the Climate Change Action Fund (CCAF).

APPENDIX A

In-Cloud Horizontal Distributions of Thermodynamic Properties

In order to obtain f_c, the mean liquid water mixing ratio, and the buoyancy in the cloud, linearized expressions are derived for the distributions of thermodynamic properties in the cloud.

The saturation water mixing ratio r^* is linearized in terms of the mixing fraction f,

$$r^* = \tilde{r}^* + \frac{dr^*}{dT}\frac{dT}{df}f, \tag{A1}$$

with the saturation vapor mixing ratio $\tilde{r}^*$ that refers to the least diluted air in the core of the cloud at the same pressure as the environment of the cloud. Similar, a linearization of the temperature in the cloud is used,

$$T = \tilde{T} + \frac{dT}{df}f. \tag{A2}$$

The temperature derivative in Eqs. (A1) and (A2) can be formulated in terms of the derivative of the moist static energy $h = c_pT + L_vr + gz$. With Eq. (8),

$$\frac{dT}{df} = \frac{h_e - \tilde{h}}{c_p + L_v\dfrac{dr^*}{dT}}. \tag{A3}$$

It is assumed that the cloud is defined at that region in which $r_t \geq r^*$, i.e. $r_t = r^*$ at $f_{\max}$. The solution of Eq. (A1) at $f = f_{\max}$ using Eq. (8) for r_t yields

$$f_{\max} = \frac{\tilde{r}_t - \tilde{r}^*}{\dfrac{dr^*}{dT}\dfrac{dT}{df} - (r_{te} - \tilde{r}_t)},$$

which can be solved using Eq. (A3) and the values of the thermodynamic properties in the core of the cloud and in the environment.

The mean liquid water mixing ratio r_{lc} and the buoyancy B_c in the cloud are calculated from

$$\psi_c = \int_0^{f_{\max}} \psi p(f)\, df,$$

with $\psi = (r_t - r^*)$ for $\psi_c = r_{lc}$ and $\psi = T(1 - r_t + 1.608r^*)$ for $\psi_c = B_c$ and using Eqs. (A1) to (A3) for the final solutions.

APPENDIX B

Cloud Ensembles

We now consider the role of the life cycle of individual clouds in the time averaged effects of ensembles of shallow cumulus clouds. In order to assess the impacts of individual clouds on ensemble mass fluxes consider the time interval $[\hat{t}, \hat{t} + \Delta t]$, where Δt is on the order of a typical time step in an AGCM, typically a few tens of minutes to an hour. An idealized individual cloud in the ensemble that is initiated at the bottom of the cloud layer at time t_0 evolves according to the equations given in section 2d if the local time is defined as the departure from the time of initiation. This idealized cloud contributes to the ensemble mass flux at each level only if $\hat{t} - \tau < t_0 < \hat{t} + \Delta t - t_*$. The mean mass flux of the cloud in the considered time interval is obtained by averaging over Δt,

$$\langle M_c \rangle = M_0 I, \tag{B1}$$

where $M_0 = \rho a_0 w_c$ and

$$I(\hat{t}, \Delta t, t_0) = \begin{cases} \dfrac{t_0 + \tau - \hat{t}}{\Delta t}, & \text{if } \hat{t} - \tau < t_0 \leq \hat{t} - t_*, \\ \dfrac{\tau - t_*}{\Delta t}, & \text{if } \hat{t} - t_* < t_0 \leq \hat{t} + \Delta t - \tau, \\ \dfrac{\hat{t} + \Delta t - t_0 - t_*}{\Delta t}, & \text{if } \hat{t} + \Delta t - \tau < t_0 < \hat{t} + \Delta t - t_*, \\ 0, & \text{otherwise.} \end{cases}$$

Further suppose all clouds in the ensemble are initiated at different times t_0 but have equal life cycles and the same properties; that is, the mean mass flux of each individual cloud is given by Eq. (B1). Let $n = dN/dt$ be the number of clouds N that are initiated per time increment. Then the mean mass flux of the ensemble is

$$\langle M_{ct} \rangle = M_0 \int_{t-\tau}^{t+\Delta t-t_*} I(t, \Delta t, t_0) n\, dt_0. \tag{B2}$$

The solution of Eq. (B2) for steady n is given by

$$\langle M_{ct} \rangle = \left(1 - \frac{t_*}{\tau}\right)\left[\frac{M_0(z)}{M_0(z_b)}\right]M_b, \qquad \text{(B3)}$$

where $\langle M_{ct} \rangle = M_b$ at cloud base and n is chosen to be

$$n = \left[\frac{M_b}{M_0(z_b)}\right]\left(\frac{1}{\tau}\right),$$

where M_b is the mass flux of the cloud ensemble at the bottom of the cloud layer.

REFERENCES

Arakawa, A., and W. H. Schubert, 1974: Interaction of a cumulus cloud ensemble with the large-scale environment, Part I. *J. Atmos. Sci.,* **31,** 674–701.

Asselin, R. A., 1972: Frequency filter for time integrations. *Mon. Wea. Rev.,* **100,** 487–490.

Betts, A. K., 1975: Parametric interpretation of trade-wind cumulus budget studies. *J. Atmos. Sci.,* **32,** 1934–1945.

——, 1982: Cloud thermodynamic models in saturation point coordinates. *J. Atmos. Sci.,* **39,** 2182–2191.

——, 1986: A new convective adjustment scheme. Part I: Observational and theoretical basis. *Quart. J. Roy. Meteor. Soc.,* **112,** 693–709.

Blyth, A. M., 1993: Entrainment in cumulus clouds. *J. Appl. Meteor.,* **32,** 626–641.

——, W. A. Cooper, and J. B. Jensen, 1988: A study of entrained air in Montana cumuli. *J. Atmos. Sci.,* **45,** 3944–3964.

Bretherton, C. S., 1993: Understanding Albrecht's model of trade cumulus cloud fields. *J. Atmos. Sci.,* **50,** 2264–2283.

——, and P. K. Smolarkiewicz, 1989: Gravity waves, compensating subsidence and detrainment around cumulus clouds. *J. Atmos. Sci.,* **46,** 740–759.

——, and Coauthors, 1999: An intercomparison of radiatively driven entrainment and turbulence in a smoke cloud, as simulated by different numerical models. *Quart. J. Roy. Meteor. Soc.,* **125,** 391–423.

Brown, A. R., 1999: The sensitivity of large-eddy simulations of shallow cumulus convection to resolution and subgrid model. *Quart. J. Roy. Meteor. Soc.,* **125,** 469–482.

——, S. H. Derbyshire, and P. J. Mason, 1994: Large-eddy simulation of stable atmospheric boundary layers with a revised stochastic subgrid model. *Quart. J. Roy. Meteor. Soc.,* **120,** 1485–1512.

Carpenter, R. L., K. K. Droegemeier, and A. M. Blyth, 1998: Entrainment and detrainment in numerically simulated cumulus congestus clouds. Part III: Parcel analysis. *J. Atmos. Sci.,* **55,** 3440–3455.

Chlond, A., 1992: Three-dimensional simulation of cloud street development during a cold air outbreak. *Bound.-Layer Meteor.,* **58,** 161–200.

——, 1994: Locally modified version of Bott's advection scheme. *Mon. Wea. Rev.,* **122,** 111–125.

Cho, H.-R., 1977: Contributions of cumulus life-cycle effects to the large-scale heat and moisture budget equations. *J. Atmos. Sci.,* **34,** 87–97.

Ciesielski, P. E., W. H. Schubert, and R. H. Johnson, 1999: Large-scale heat and moisture budgets over the ASTEX region. *J. Atmos. Sci.,* **56,** 3241–3261.

Cuijpers, J. W. M., and P. G. Duynkerke, 1993: Large-eddy simulation of trade-wind cumulus clouds. *J. Atmos. Sci.,* **50,** 3894–3908.

Emanuel, K. A., 1991: A scheme for representing cumulus convection in large-scale models. *J. Atmos. Sci.,* **48,** 2313–2335.

——, and M. Živković-Rothman, 1999: Development and evaluation of a convection scheme for use in climate models. *J. Atmos. Sci.,* **56,** 1766–1782.

Esbensen, S., 1978: Bulk thermodynamic effects and bulk properties of small tropical cumuli. *J. Atmos. Sci.,* **35,** 826–837.

Fraedrich, K., 1974: Dynamic and thermodynamic aspects of the parameterization of cumulus convection: Part II. *J. Atmos. Sci.,* **31,** 1838–1849.

Grinnell, S. A., C. S. Bretherton, D. E. Stevens, and A. M. Fraser, 1996: Vertical mass flux calculations in Hawaiian trade cumulus from dual-Doppler radar. *J. Atmos. Sci.,* **53,** 1870–1886.

Holland, J. Z., and E. M. Rasmusson, 1973: Measurements of atmospheric mass, energy, and momentum budgets over a 500-kilometer square of tropical ocean. *Mon. Wea. Rev.,* **101,** 44–55.

Jiang, H., and W. R. Cotton, 2000: Large eddy simulation of shallow cumulus convection during BOMEX: Sensitivity to microphysics and radiation. *J. Atmos. Sci.,* **57,** 582–594.

Johnson, R. H., and X. Lin, 1997: Episodic trade wind regimes over the western Pacific warm pool. *J. Atmos. Sci.,* **54,** 2020–2034.

Kogan, Y. L., M. P. Khairoutdinov, D. K. Lilly, Z. N. Kogan, and Q. Liu, 1995: Modeling of stratocumulus cloud layers in a large eddy simulation model with explicit microphysics. *J. Atmos. Sci.,* **52,** 2923–2940.

Kuo, H. L., 1965: On the formation and intensification of tropical cyclones through latent heat release by cumulus convection. *J. Atmos. Sci.,* **22,** 40–63.

Lewellen, D. C., W. S. Lewellen, and S. Yoh, 1996: Influence of Bowen ratio on boundary-layer cloud structure. *J. Atmos. Sci.,* **53,** 175–187.

Lin, C., and A. Arakawa, 1997a: The macroscopic entrainment processes of simulated cumulus ensemble. Part I: Entrainment source. *J. Atmos. Sci.,* **54,** 1027–1043.

——, and ——, 1997b: The macroscopic entrainment processes of simulated cumulus ensemble. Part II: Testing the entraining-plume model. *J. Atmos. Sci.,* **54,** 1044–1053.

MacVean, M. K., 1993: A numerical investigation of the criterion for cloud-top entrainment instability. *J. Atmos. Sci.,* **50,** 2481–2495.

Moeng, C.-H., 1984: A large-eddy simulation model for the study of boundary layer turbulence. *J. Atmos. Sci.,* **41,** 2052–2062.

——, 1986: Large-eddy simulation of a stratus-topped boundary layer. Part I: Structure and budgets. *J. Atmos. Sci.,* **43,** 2886–2900.

Morton, B. R., 1997: Discrete dry convective entities: I Review. *The Physics and Parameterization of Moist Atmospheric Convection,* R. K. Smith, Ed., Kluwer, 143–173.

Nitta, T., 1975: Observational determination of cloud mass flux distributions. *J. Atmos. Sci.,* **32,** 73–91.

——, and S. Esbensen, 1974: Heat and moisture budget analyses using BOMEX data. *Mon. Wea. Rev.,* **102,** 17–28.

Ogura, Y., and H. R. Cho, 1973: Diagnostic determination of cumulus cloud populations from observed large-scale variables. *J. Atmos. Sci.,* **30,** 1276–1286.

Paluch, I. R., 1979: The entrainment mechanism in Colorado cumuli. *J. Atmos. Sci.,* **36,** 2462–2478.

Raga, G. B., J. B. Jensen, and M. B. Baker, 1990: Characteristics of cumulus band clouds off the coast of Hawaii. *J. Atmos. Sci.,* **47,** 338–355.

Raymond, D. J., and A. M. Blyth, 1986: A stochastic model for nonprecipitating cumulus clouds. *J. Atmos. Sci.,* **43,** 2708–2718.

Siebesma, A. P., 1998: Shallow cumulus convection. *Buoyant Convection in Geophysical Flows,* E. J. Plate et al., Eds., Kluwer Academic, 441–486.

——, and W. M. Cuijpers, 1995: Evaluation of parametric assumptions for shallow cumulus convection. *J. Atmos. Sci.,* **52,** 650–666.

——, and A. A. M. Holtslag, 1996: Model impacts of entrainment and detrainment rates in shallow cumulus convection. *J. Atmos. Sci.,* **53,** 2354–2364.

Simpson, J., and V. Wiggert, 1969: Models of precipitating cumulus towers. *Mon. Wea. Rev.,* **97,** 471–489.

Soong, S.-T., and Y. Ogura, 1976: A determination of the trade-wind cumuli population using BOMEX data and an axisymmetric cloud model. *J. Atmos. Sci.,* **33,** 992–1007.

Squires, P., 1958: Penetrative downdraughts in cumuli. *Tellus,* **10,** 381–389.

Stevens, D. E., and C. S. Bretherton, 1999: Effects of resolution on the simulation of stratocumulus entrainment. *Quart. J. Roy. Meteor. Soc.,* **125,** 425–439.

Stith, J. L., 1992: Observations of cloud-top entrainment in cumuli. *J. Atmos. Sci.,* **49,** 1334–1347.

Taylor, G. R., and M. B. Baker, 1991: Entrainment and detrainment in cumulus clouds. *J. Atmos. Sci.,* **48,** 112–121.

Tiedtke, M., 1989: A comprehensive mass flux scheme for cumulus parameterization in large-scale models. *Mon. Wea. Rev.,* **117,** 1779–1800.

Yanai, M., S. Esbensen, and J. H. Cho, 1973: Determination of bulk properties of tropical cloud clusters from large-scale heat and moisture budgets. *J. Atmos. Sci.,* **30,** 611–627.

Yau, M. K., 1979: Perturbation pressure and cumulus convection. *J. Atmos. Sci.,* **36,** 690–694.